RICE UNIVERSITY

COLLISIONS OF HIGHLY EXCITED XENON ATOMS

by

GREG WILLIAM FOLTZ

A THESIS SUBMITTED
IN PARTIAL FULFILLMENT OF THE
REQUIREMENTS FOR THE DEGREE OF

MASTER OF SCIENCE

THESIS DIRECTOR'S SIGNATURE:

R. F. Stebbings

HOUSTON, TEXAS

APRIL, 1976

ABSTRACT

Collisions of Highly Excited Xenon Atoms

by

Greg William Foltz

The collisional ionization of xenon high Rydberg atoms by various target gases is investigated. Ground state xenon atoms are excited by an electron impact-photoexcitation method to the selected high Rydberg states $5p^5(^2P_{3/2})nf[3/2]_1$ where n has a value between 25 and 40. Absolute rate constants are measured for the ionization of these atoms in collision with CCl_4, H_2O, NH_3, H_2S, SO_2, CCl_3F, and CCl_2F_2 under conditions of zero electric field and small electric fields. The experimental method is discussed and the results are compared with other experiments and with theory.

ACKNOWLEDGEMENTS

It is with pleasure that I acknowledge the people and organizations who made this thesis possible. I am indebted to my advisor, Dr. Ron Stebbings, who has given constant guidance, advice and encouragement throughout the work. The valuable assistance of Dr. Barry Dunning is also much appreciated.

Dr. Colin Latimer and Dr. Phil West, with whom I worked in the lab, provided constant help and deserve much credit for the success of this work. I have also benefited from helpful discussions with Dr. Ken Smith and Tom Cook.

The financial support provided by the Robert A. Welch Foundation and the National Science Foundation under contract number MPS 74-11690 is appreciated.

I thank my parents, Dr. and Mrs. Floyd Foltz, for their help in making this goal in my education attainable.

Finally, I would like to acknowledge Chris Dunning and John Beasley for their assistance in the preparation of the manuscript.

TABLE OF CONTENTS

CHAPTER 1

Introduction

A high Rydberg atom may be defined as an atom in which one of the outer, valence electrons is excited to a state having a large principal quantum number, n. Such atoms have energies close to the ionization limit, large radii and geometric cross sections, and are quite fragile. High Rydberg atoms are also long-lived and can therefore play prominent roles in processes occurring in a number of environments. Examples are interstellar gaseous nebulae, laboratory plasmas, and flames.

In order to thoroughly understand the atomic processes occurring in gaseous nebulae, it is necessary to have a model which accurately gives the observed spectral line intensities of the clouds. This requires a knowledge of how the various energy levels of the atoms are populated. In the environment of a gaseous nebula there is a wide variety of interactions which influence these populations. The processes include

$$H(n) + h\nu \rightarrow H^+ + e \qquad \text{photoionization} \qquad (1\text{-}1)$$

$$H^+ + e \rightarrow H(n) + h\nu \qquad \text{radiative recombination} \qquad (1\text{-}2)$$

$H^+ + e + e \rightarrow H(n) + e$	three-body recombination	(1-3)
$H(n) \rightarrow H(n') + h\upsilon$	radiative cascade	(1-4)
$H(n) + e \rightarrow H^+ + e + e$	collisional ionization	(1-5)
$H(n) + e \rightarrow H(n') + e$	n changing collisions	(1-6)
$H(n) + h\upsilon \rightarrow H(n') + 2h\upsilon$	stimulated emission	(1-7)

where n is the principal quantum number of the level involved. The cross section for a given reaction needs to be known as it is a measure of the importance that reaction has in determining the occupation of a level. In the case of the radio recombination lines of the interstellar hydrogen regions the energy levels lie at large n values and the above reactions involve highly excited atoms.[1-3]

The role of high Rydbergs in plasmas in general (including laboratory plasmas) is quite similar to their role in the specific case of the gaseous nebulae. In tenuous plasmas the rate of populating a state in a given atom or ion is governed mainly by radiative processes while in dense plasmas this rate is determined predominantly by collisions. In the intervening case both types of processes are important and one must consider the whole spectrum of possible interactions such as those given above in Eqns. (1-1) - (1-7) for the astrophysical situation. Bates, Kingston and McWhirter[4] have included interactions

(1-1) - (1-6) in calculations of the overall rate coefficient for both optically thin and thick plasmas. McWhirter and Hearn[5] have determined values for the population of ionic energy levels in plasmas.

High Rydberg atoms and molecules may also be of importance in the design of neutral particle injection devices for magnetic confinement-type fusion reactors due to the smaller Lorentz force required to ionize a highly excited state as compared to the ground or lower lying state.[6]

It is a well established fact that flames contain positive ions and free electrons. One process currently thought to produce this ionization in the case of metal impurities in a flame is

$$A^* + M(J') \rightarrow A^+ + M(J) + e \qquad J < J' \qquad (1\text{-}7)$$

where A* is an excited state of impurity atom A and M(J) is a rotationally excited molecule M.[7,8] The states of A* can range from low-lying ones to levels near the ionization continuum. The ionization mechanism is considered to be a rotational de-excitation of M(J') with the released energy going to liberate the excited electron.

Due to their excitation close to the ionization limit, high Rydberg atoms have recently been shown to be useful in the process of isotope separation.[9]

CHAPTER 2

Background

High Rydberg atoms were first detected in the laboratory as products of the electron excitation of rare gases in experiments conducted by Čermák and Herman[10] and by Melton and Hamill.[11] This chapter reports on the basic nature of high Rydberg atoms and on high Rydberg work accomplished prior to the present investigation.

A good idea of the size and energy level structure of a high Rydberg atom can be obtained by appealing to the hydrogen atom for which these properties, as functions of n, can be determined exactly. It is well known from wave mechanics that the expectation value for the radius, r, of a hydrogenic wave function is

$$\langle r_{n\ell m} \rangle = \frac{a_o}{2} [3n^2 - \ell(\ell + 1)]. \qquad (2\text{-}1)$$

This gives a mean geometric cross section of $\pi \langle r_{n\ell m} \rangle^2$ for the atom. It is also well established that the energy of a given state having principal quantum number n is (neglecting spin-orbit and other relativistic corrections)

$$E_n = -\frac{R}{n^2} \qquad (2\text{-}2)$$

where R is the Rydberg constant. For a hydrogen atom whose electron has the quantum numbers n = 50 and ℓ = 3, the above equations yield: $\langle r \rangle \sim 2000$ Å, $\pi \langle r \rangle^2 \sim 1.2 \times 10^7$ Å^2, E = -5.44 meV, and a separation between the adjacent energy levels of about 0.22 meV. As is readily seen, highly excited hydrogen atoms are very large and have energies close to the ionization limit.

Due to the Rydberg electron's large value of n and the fact that the density of states at this value of n is large, the Bohr correspondence principle may be invoked which allows the Rydberg electron to be viewed as a classical particle moving about the ion core in a Kepler type orbit. Furthermore, if the Rydberg electron has sufficient angular momentum so that it does not appreciably penetrate the core, then the core will always look small to the Rydberg electron and the core electrons will effectively screen all but one nuclear charge from this electron. Therefore the high Rydberg will be hydrogenic in nature.

2.1 Production of high Rydberg species.

There are a variety of techniques which may be used to produce high Rydberg species in the laboratory. Collisional excitation of atoms by electron impact results

in a certain fraction of highly excited atomic states.[10-23] Electron collisions with molecules can also produce high Rydberg atoms.[12,21,23-32] The mechanism thought to be operating here is first excitation of the molecule to a molecular high Rydberg state having a dissociative ion core, followed rapidly by dissociation in which one of the atoms retains the Rydberg electron in a highly excited state.[24]

High Rydberg atoms can also be produced via electron transfer (also called capture) to positive ions;[33-36] however, due to the large energy defect for the process this method requires fast positive ion beams to make it efficient. The fast beam requirement limits this production technique to uses in merged beam collision work,[36] studies of collisions involving large relative velocities between the interacting particles, and to injection devices for magnetically confined plasmas.

Both of the production techniques, electron impact excitation and electron transfer, suffer from the inability to produce high Rydbergs in states that are well defined with respect to the quantum numbers n and ℓ of the excited electron. Following production by the above methods some n selection of the high Rydbergs has been obtained by various time of flight and field ionization

techniques.[16,30,31] Nevertheless, the value of ℓ remains undefined.

This selection deficiency can be solved by the use of optical excitation since resonant transitions to well defined states can be accomplished with sufficiently monochromatic sources of light. This method was first applied in the excitation of high lying states of the rare gases by Huffman and Katayama[37] and by Chupka.[38] The use of tunable lasers to optically produce specific high Rydberg states is growing in popularity.[39-42] A two-step process has been used to excite high Rydberg xenon atoms where electron impact populates the $^3P_0$ metastable state from which optical transitions to selected high Rydberg states are carried out with a tunable laser.[43-45] This is the production process employed in the present work and it will be discussed in detail in Chapter 3. In another two-step technique[46] fast hydrogen atoms in the 2s state, formed by charge transfer in H_2, have been photoexcited to selected high lying n states with a laser tuned by the Doppler effect.

Although optical excitation can produce individual high Rydberg states, it has the disadvantage of being able to populate only states with small ℓ. This is due to the parity selection rule for dipole transitions and

the fact that the initial state from which the transition is made is usually a low lying state. However, it has been shown recently[42] that this problem may be overcome by allowing the transition to occur in the presence of an electric field.

2.2 Lifetimes of high Rydbergs.

Highly excited atoms have long lifetimes against radiative decay. These lifetimes can be explained physically in the following way. The total dipole transition rate from a given state, n, to lower states, n', is given by the Einstein $A_{nn'}$, coefficient summed over all allowed lower states. This total transition rate is just the reciprocal of the lifetime, τ_n, of the state n. Thus

$$\tau_n = [\Sigma_{n'} A_{nn'}]^{-1} \qquad (2\text{-}3)$$

where $A_{nn'}$ is given by

$$A_{nn'} = \frac{64\,\pi^4\,\upsilon_{nn'}^3}{3h}\,(\langle\psi_{n\ell m}|e\vec{r}|\psi_{n'\ell'm'}\rangle)^2 . \qquad (2\ 4)$$

Here $\upsilon_{nn'}$ is the frequency of the transition and the quantity in the parentheses is the matrix element of the dipole operator, $e\vec{r}$, between the initial and final

states. For a high Rydberg state the transition rate to a neighboring state is small because $\upsilon_{nn'}$ is small; the transition rate to a low lying state is also small since the matrix element (i.e., overlap) between the two states is small. Consequently, τ_n is long for all transitions. The quantum theoretical analysis for hydrogen[47] gives the result that, for a given value of ℓ, the lifetime is proportional to n^3. The hydrogen calculations[47] further show that of the ℓ sublevels the p state has the shortest lifetime for a given n and that the lifetime averaged over all ℓ states scales as $n^{4.5}$. For atoms other than hydrogen, quantum defect theory predicts that the lifetime for a given value of ℓ should still be proportional to the cube of the atom's principal quantum number where this principal quantum number is no longer the integer n but rather it is n_{eff} the "effective" quantum number.[39] Experimental measurements have been made of sodium[39] and xenon[44,48] high Rydberg lifetimes and they give confirmation of the expected hydrogenic behavior. Stebbings et al.[44] have also found that lifetimes of xenon high Rydbergs are lengthened when the atoms are placed in an electric field. They attributed this phenomenon to an induced mixing of the angular momentum states by the electric field and this leads

to longer lifetimes as has been mentioned above for hydrogen.

2.3 Field ionization of high Rydbergs.

Application of an electric field to a high Rydberg atom produces shifts in the energies of the excited states and may remove degeneracies within the states. This Stark shift is shown schematically for a given state in Fig. (2-1) which pictures the unperturbed potential well of the atom (at large n) on the left followed by the effective potential seen by the Rydberg electron after the application of an electric field. It is seen from the figure that a potential maximum exists on the right hand side of the perturbed well and is denoted V_{max}. Classically if an electron lies in a state above V_{max} it will leave the atomic core (ionization) while if it lies below V_{max} it will remain bound indefinitely to the core. The value of V_{max}, the classical ionization threshold, is given by

$$E_c = \frac{R}{4e^3 n^4} \quad . \qquad (2\text{-}5)$$

However, from the quantum mechanical viewpoint, tunnelling through the barrier by the Rydberg electron is

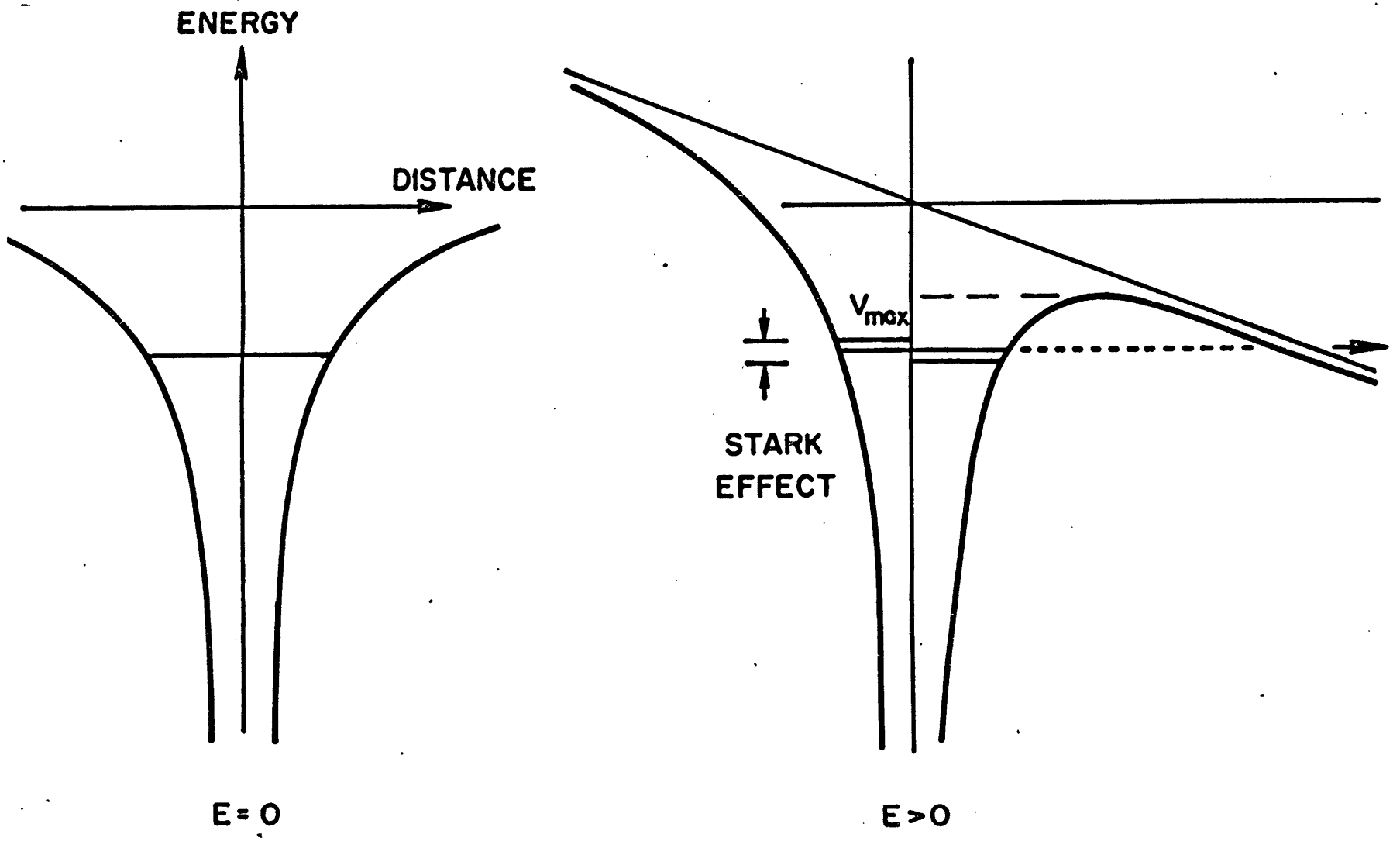

Figure (2-1) Potential well seen by the Rydberg electron: unperturbed on left; in an applied electric field on right.

also possible for states lying below V_{max} as shown in the figure. Tunnelling will contribute to the overall ionization rate for all states in which the time required to pass through the barrier is shorter than the radiative lifetime. Thus the quantum mechanical ionization threshold occurs at a potential below V_{max}. Calculations of the ionization rate of hydrogen[49] reveal that this rate for a given n is a rapidly increasing function of the strength of the applied electric field. This implies a sharp threshold for ionization of a given state and the ability to distinguish between different states by using the field appropriate to each state. This has been experimentally proven[41,44,49] and an example of this threshold phenomenon is shown in Fig. (2-2) for the 28f state of xenon.[44] A critical field, E_c, can be defined such that for fields below E_c essentially none of the atoms are ionized while for fields above E_c all of the atoms are ionized. Thus field ionization can be used as an absolute detection technique. Critical field values for selected high lying states in xenon have been measured by Stebbings et al.[44] and compared to hydrogen. Again the hydrogenic nature of the high Rydberg atoms is revealed.

Ionization of high Rydberg atoms can occur near metal surfaces which, for atoms having thermal energies, appears

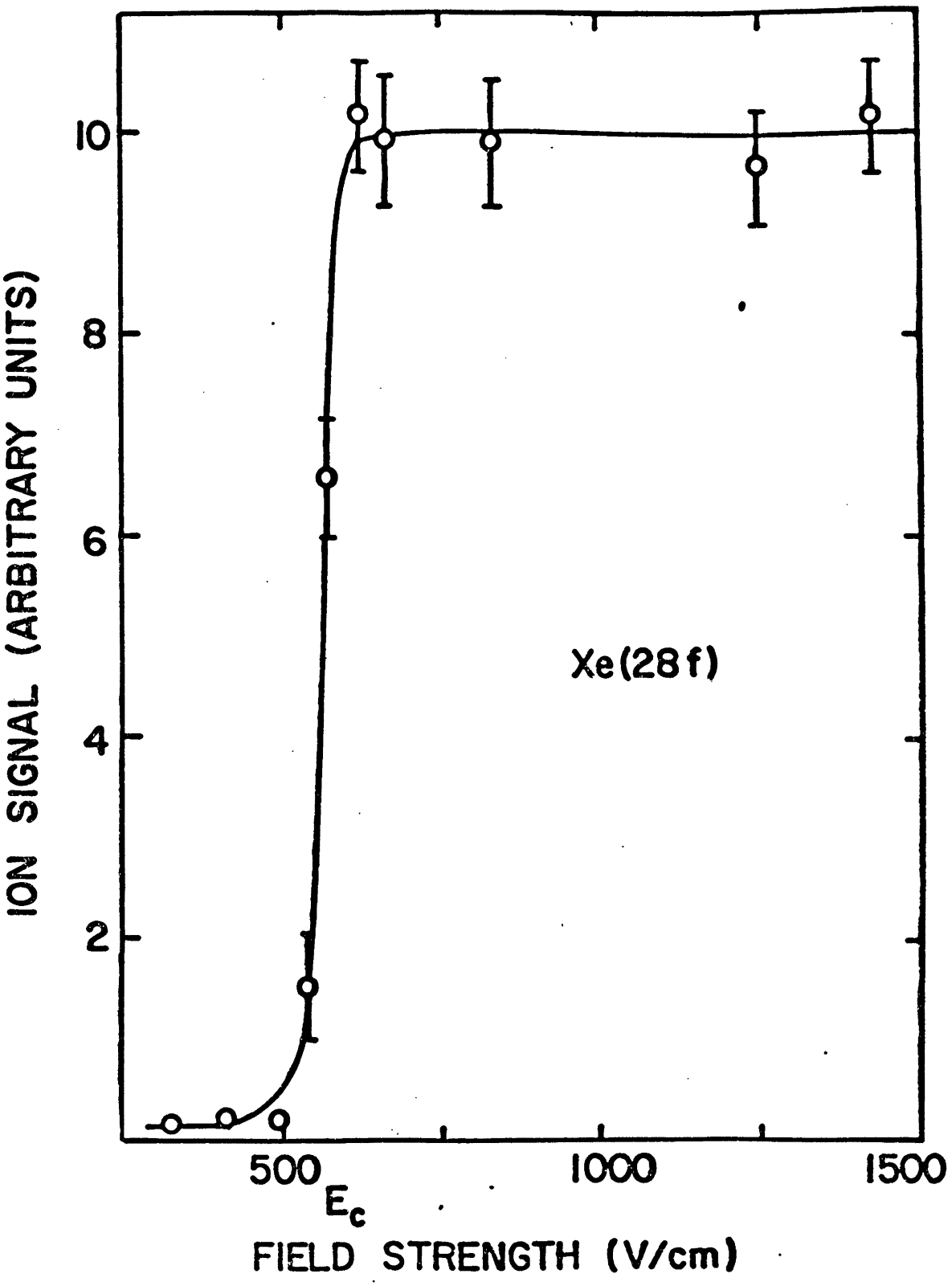

Figure (2-2) Xe^+ ion signal produced by field ionization versus the applied electric field strength.

formally in the theory to resemble field ionization.[50] The process has also been studied experimentally.[15]

Also in regard to ionization of highly excited atoms as a result of the presence of a field, the multiphoton ionization of high Rydberg hydrogen atoms is being examined using microwave frequencies.[35,46]

2.4 Collisional phenomena involving high Rydbergs.

Highly excited atoms can enter into a wide variety of collisional processes and, as stated in Chapter 1, this results in their being important in many environments. Both chemiionization involving high Rydbergs and molecules

$$A^{**} + BC \rightarrow A + BC^{+} + e \qquad (2\text{-}6a)$$

$$\rightarrow A + B + C^{+} + e \qquad (2\text{-}6b)$$

$$\rightarrow ABC^{+} + e \qquad (2\text{-}6c)$$

$$\rightarrow AB^{+} + C + e \qquad (2\text{-}6d)$$

and collisional ionization of high Rydbergs by molecules

$$A^{**} + BC \rightarrow A^{+} + (BC + e) \qquad (2\text{-}7)$$

where A** is the high Rydberg and BC is a target molecule, were the first processes used in the detection of these highly excited atoms.[10,11]

Penning and dissociative ionization [(2-6a) and (2-6b) above, respectively] of C_2H_4 by highly excited rare gases have been observed[10,12] while the molecular ions HeH_2^+ and ArH^+ have been attributed to collisions between high Rydberg helium and argon atoms respectively and molecular hydrogen.[12,14] Hotop and Niehaus[17] have studied chemiionization processes between hydrogen and highly excited argon and krypton and have estimated a cross section for the production of ArH^+ to be $\sim 10^{-14} cm^2$.

Collisional ionization of high Rydbergs has been observed in a number of investigations[11,16,19-22,25,29,38,45] in which the target species were dipolar molecules and thermal electron attaching molecules. Early experimental work[16,19] in which the states of the high Rydbergs were ill-defined has produced cross sections of $\sim 10^{-12}$ to $\sim 10^{-13}$ cm^2 for these processes and this is in agreement with present theoretical predictions. Recently in this laboratory,[45] absolute rate constants and cross sections have been measured for the collisional ionization process

$$Xe(nf) + SF_6 \rightarrow Xe^+ + (SF_6 + e) \qquad (2\text{-}8)$$

where the xenon atoms were in well defined high Rydberg states with $\ell = 3$ and $25 \leq n \leq 40$. It was also found in this work that the rate constant for the above process

is smaller when the collisions occur in a small residual electric field than when the collisions occur in a field free region. A more complete discussion of this work and other collisional ionization work, both experimental and theoretical, will be given in Chapter 4 along with the results of the present investigation.

Gallagher et al.[40] have found that collisions between sodium atoms in well defined nd states (principal and angular momentum quantum numbers respectively of the Rydberg electron) and rare gas atoms result in a lengthening of the fluorescent lifetimes of the sodium states. The lifetimes obtained were in good agreement with the $n^{4.5}$ dependence mentioned earlier. From this it was inferred that the collisions change the value of ℓ in the original atoms and produce sodium atoms in $n\ell$ states where ℓ can take on any value greater than or equal to 2, which is consistent with the value of n.

2.5 Detection techniques for high Rydbergs.

From what has been said so far it is apparent that there are many different techniques for the detection of high Rydbergs. Field ionization has been the most popular method used and has the advantage of giving an absolute measurement. Collisional ionization, chemiionization, and

multiphoton ionization have all been employed but they require knowledge of absolute cross sections in order to be absolute detectors. Fluorescence from high Rydberg states has been used but is not very efficient for high n states because of the long lifetimes involved. Finally, ionization of highly excited species next to a metal surface has been used extensively but, as far as the writer is aware, the efficiency of this process is not definitely known.

2.6 Purpose of present work.

The value of understanding the collisional behavior of highly excited atoms has been pointed out in Chapter 1. It is the purpose of the present experiment to continue the high Rydberg investigations initiated in this laboratory by Stebbings et al.[44] and in particular to extend the collisional ionization work of West et al.[45] This thesis reports the measurement of absolute rate constants and cross sections for the collisional ionization of selected high Rydberg states of xenon with the dissociative electron attaching gas CCl_4 and with the dipolar gases H_2O, NH_3, H_2S, SO_2, and CCl_2F_2. Also, CCl_3F, which has a significant cross section for free electron attachment and has a dipole moment, is examined. For several of the

targets, the effect of an electric field on the rate constants is investigated. The results are compared with other experimental data and with theory.

CHAPTER 3

Apparatus and Procedure

3.1 Expression for collisional ionization rate constant.

The experimental technique adopted for the measurement of the cross sections for collisional ionization of xenon high Rydbergs can be referred to as a beam-cell method. The target gas is confined in the cell while the beam contains the high Rydberg atoms. In the usual beam-cell technique the beam of incident particles is exponentially attenuated as it passes through the cell due either to collisions which scatter the incident particles out of the beam, or to reactive collisions which change the character of the incident particles. In the simplest case, when a monoenergetic beam of particles having velocity v is incident on a stationary target, this attenuation is described by

$$N(z) = N_o \exp[-n\,\sigma(v)\,z]. \qquad (3\text{-}1)$$

Here z is the path length of the beam through the target and, in this case, is equal to the actual distance that the beam travels through the cell. The target density is specified by n, $\sigma(v)$ is the total cross section for loss of incident particles from the beam at the velocity v,

and N_o and N(z) are the number densities of incident particles entering the cell and at the distance z into the cell respectively. Since z = vt, where t is the time required to travel the distance z, Eqn. (3-1) can be rewritten as

$$N(t) = N_o \exp[-n\,\sigma(v)\,v\,t] \tag{3-2}$$

and, due to v being a constant, the quantity $\sigma(v)\,v$ exactly equals the rate constant k. Thus

$$N(t) = N_o \exp[-n\,k\,t]. \tag{3-3}$$

In the present work both the high Rydberg atoms in the beam and the target gas have certain velocity distributions $\mathcal{F}(\vec{v}_1)$ and $\mathcal{F}(\vec{v}_2)$ respectively. Nevertheless, Eqn. (3-3) may still be used where now the rate constant is given by

$$k = \iint \sigma(v_r)\, v_r\, \mathcal{F}(\vec{v}_1)\, \mathcal{F}(\vec{v}_2)\, d^3v_1\, d^3v_2. \tag{3-4}$$

In this expression v_r is the relative velocity between the high Rydberg atoms and the target gas molecules.

$$v_r^2 = v_1^2 + v_2^2 - 2v_1v_2\cos\theta \tag{3-5}$$

where θ is the angle between the velocity vectors $\vec{v}_1$ and $\vec{v}_2$.

If the experimental conditions are such that nkt $\ll$ 1, the target is called a "thin target" and very few

collisions occur causing only a small beam attenuation. Consequently the exponential in Eqn. (3-3) may be expanded to first order terms giving

$$N(t) = N_o(1 - nkt) \tag{3-6}$$

from which follows

$$S(t) = N_o nkt \tag{3-7}$$

where $S(t) = N_o - N(t)$ is the number of high Rydbergs lost due to collision processes.

One further modification of Eqn. (3-7) is required in order to be able to handle an experiment involving high Rydbergs. The derivation of Eqn (3-7) is based upon the condition that all losses of incident particles from the beam are due to collisions whose probability of occurrence is contained in k. This excludes the possibility of natural decay and requires the particles to have an infinite lifetime. Such a situation does not exist with high Rydberg atoms, which, although long-lived, do have finite lifetimes as discussed in Chapter 2. Consequently as the high Rydbergs travel through the target gas, they will be lost from the beam as a result both of collisions (characterized by a rate constant k) and of radiative decay (characterized by a natural lifetime τ). The

modification of Eqn. (3-7) to account for this radiative decay contribution to the overall loss essentially requires the replacement of the real time, t, in the equation with an "effective time," t_{eff}, which is a function of both t and τ. This expression for t_{eff} is[51]

$$t_{eff} = \tau(1 - e^{-t/\tau}). \qquad (3\text{-}8)$$

It is seen that t_{eff} is always less than t for finite lifetimes. This expresses the fact that in a real time t the average distance traveled by an ensemble of high Rydberg atoms having velocity v is shorter than that traveled by non-decaying particles having the same velocity. As t goes to infinity, t_{eff} goes to τ which indicates that the maximum collision time available is dictated by τ. It is also seen from Eqn. (3-8) that as τ goes to infinity, t_{eff} goes to t, as it should. Using t_{eff} in Eqn. (3-7) gives

$$S(t) = N_o\, nk\tau(1 - e^{-t/\tau}). \qquad (3\text{-}9)$$

Finally, for the present experiment, if S(t) is allowed to contain only those high Rydbergs, Xe**, lost through collisional ionization with the target gas BC

$$Xe^{**} + BC \rightarrow Xe^{+} + (BC + e) \qquad (3\text{-}10)$$

instead of being the number of high Rydbergs lost due to all collisional processes, then k in Eqn. (3-9) is the rate constant, k_c, for the interaction (3-10) only. In such a case S(t) equals the number of Xe^+ ions produced assuming there is no other process creating Xe^+. Solving for this collisional ionization rate constant, k_c, in Eqn. (3-9) gives the expression

$$k_c = \frac{S(t;Xe^+)}{N_o\, n\, \tau(1 - e^{-t/\tau})} \cdot \qquad (3\text{-}11)$$

It is seen that the rate constant for collisional ionization of xenon high Rydberg atoms can be determined from Eqn. (3-11) if, for a given reaction period t, the remaining quantities on the right of the equation can be measured. The rest of this chapter will deal with the experimental determination of these quantities.

3.2 Basic experimental requirements.

The essential features of the experiment are (1) use of a high vacuum environment in which the collision process can occur, (2) preparation of a beam containing xenon high Rydberg atoms and a system which detects the absolute number of these atoms produced, (3) arrangement of a gas cell through which the high Rydberg beam passes

and which confines the target gas at a known absolute pressure, and (4) a means for extracting and counting the absolute number of Xe^+ ions produced in the collision process (3-10).

3.3 Vacuum system.

The high vacuum requirement is satisfied by a versatile crossed beams apparatus shown schematically in Fig. (3-1), which can function in a beam-cell configuration. The overall vacuum is maintained by water-cooled, oil diffusion pumps backed by mechanical rotary pumps. In addition, the apparatus is divided into a number of chambers by vacuum walls enabling it to be differentially pumped so as to attain a lower background pressure in the interaction region than at the xenon beam source. A problem with both mechanical and diffusion pumps is that pump oil vapors tend to make their way into the region that the pump is evacuating (called "backstreaming"). For diffusion pumps, this problem can be combatted by placing, at the input port of the pump, a water baffle in which cold surfaces onto which the oil vapor may condense are maintained by circulating water. A more effective device, the liquid nitrogen cold trap in which cold surfaces are maintained by using liquid nitrogen,

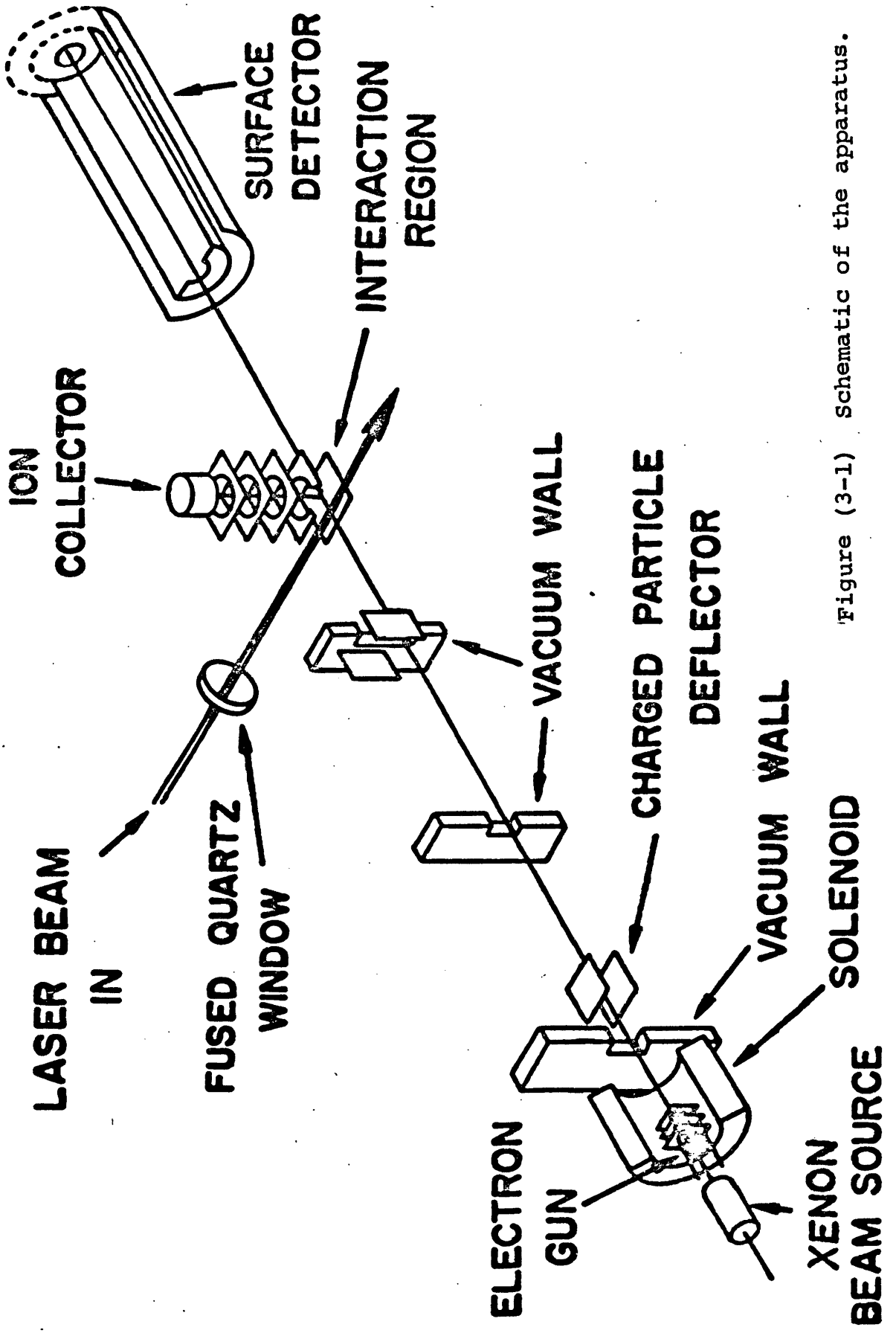

Figure (3-1) Schematic of the apparatus.

may be employed when no pump oil backstreaming can be permitted and/or when cryopumping of other condensable vapors such as water is desired. Water baffles prevent diffusion pump oil from backstreaming into the vacuum chambers on all diffusion pumps except the pump on the interaction region where a liquid nitrogen cold trap is used. Zeolite traps are located at the input ports of the mechanical pumps to stop backstreaming mechanical pump oil from entering the backing pump lines (vacuum tube connections between the output ports of the diffusion pumps and the input ports of the mechanical pumps). These traps are chambers containing the material Zeolite which absorbs the pump oil vapor. The nominal background pressure in the interaction region is about 1×10^{-7} torr.

3.4 Formation of xenon high Rydberg atoms.

The formation of the high Rydberg beam is accomplished in a two-step process shown schematically in Fig. (3-2). Ground state xenon atoms are initially excited to the metastable levels by electron impact and are then further excited to a selected high Rydberg state by a tunable dye laser. The details of this process follow.

Xenon gas at room temperature is allowed to effuse through a multichannel glass array which produces a

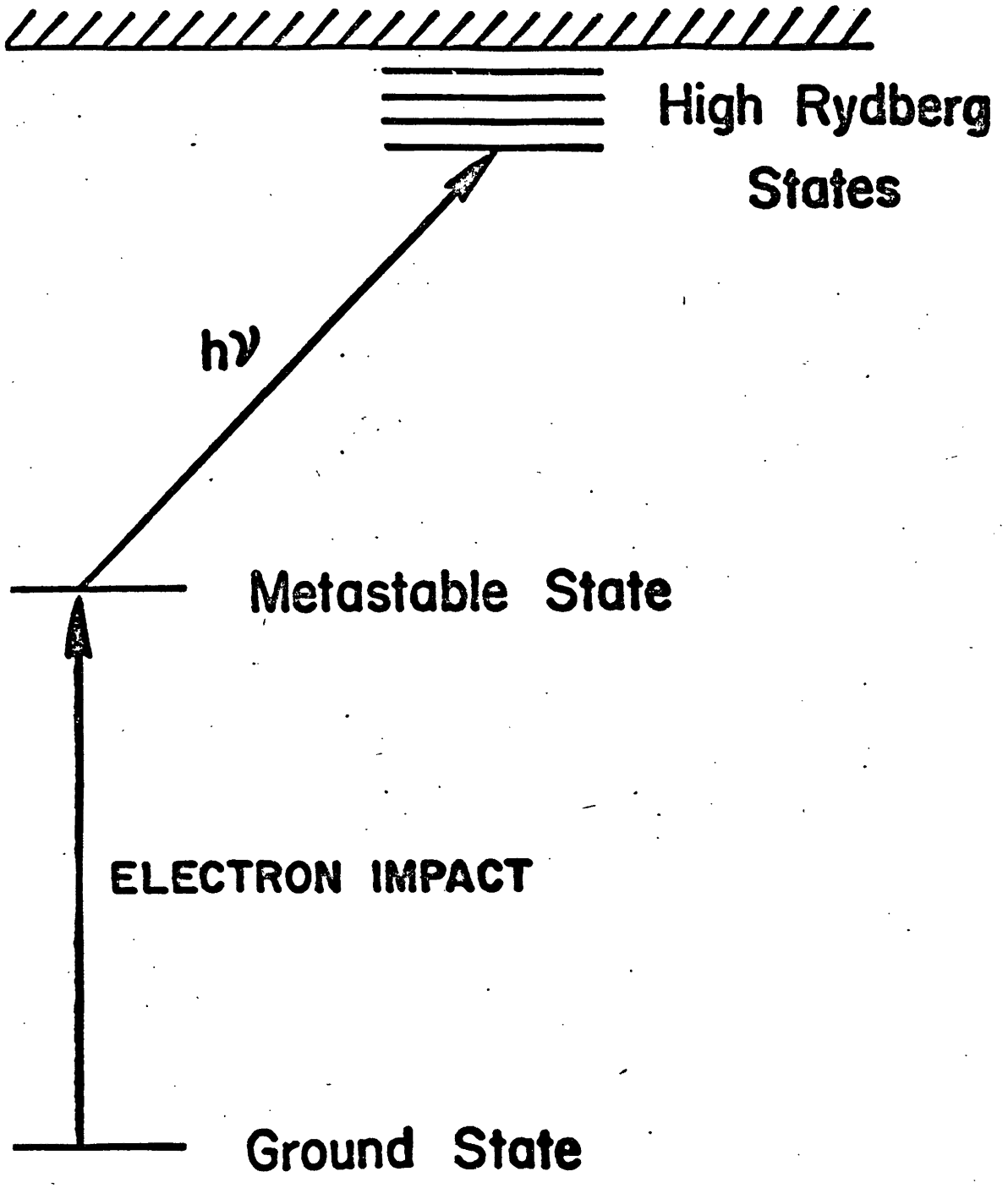

Figure (3-2) Generalized term diagram showing the two-step high Rydberg production.

moderately well directed beam of ground state xenon. (The multichannel array consists of a large number of tubes having a given length and a very small diameter, which are attached together in parallel.) The beam is further spatially defined by passing it through an aperture immediately after the array. Electrons, produced by thermal emission from a tungsten wire filament and accelerated through a potential difference, are confined by a magnetic field to travel coaxially with the xenon beam [see Fig. (3-1)]. The magnetic field is produced by a three segment solenoid. Collisions between the electrons and the xenon atoms produce both excitation and ionization of the atoms. A fraction of the excited states produced consists of the xenon metastable states which are given in the j,ℓ coupling scheme by $5p^5(^2P_{3/2})6s[3/2]_2$ and $5p^5(^2P_{1/2})6s'[1/2]_0$. The corresponding LS coupling notations are $^3P_2$ and $^3P_0$ respectively and, although less appropriate descriptions, they are more convenient to use. The $^3P_2$ state lies at 8.32 eV above the ground state while the $^3P_0$ energy is 9.45 eV. Charged particles are confined to the excitation region by appropriately biased grids while the neutral component of the beam continues toward the interaction region. Radiative decay of all excited states except the metastable and any very

high energy states occurs in the time of flight of the atoms to the interaction region. A large potential difference applied across a pair of plates just before the interaction region [see Fig. (3-1)] quenches the high lying states by field ionization. At the interaction region the beam contains only metastable and ground state xenon. The metastable content of the beam is monitored by secondary electron ejection from a surface just past the interaction region. Secondary electron ejection is the process in which an incident particle liberates a certain number of electrons from a surface when it strikes that surface. The required energy may come from the internal or translational energy of the incident particle. The current produced from the secondary electrons is nominally about 5×10^{-12} amps. This corresponds to a flux of metastables in the beam of $5 \times 10^{-12} (e\gamma)^{-1}$ metastables/sec where e is the electronic charge in coulombs and γ is the secondary electron ejection coefficient (number of electrons ejected per incident metastable).

The optical excitation to the high Rydberg states is accomplished by irradiating the xenon beam with the output of a pulsed nitrogen pumped tunable dye laser. The nitrogen laser essentially consists of a bank of capacitors which discharge, when a spark gap is fired, into a set of

low inductance, high capacitance cables connected to the nitrogen plasma tube. The cables charge up until breakdown of the nitrogen occurs and then, due to their low inductance, rapidly discharge into the nitrogen creating an intense discharge. This discharge produces the required population inversion in the nitrogen and lasing action follows. The output of the nitrogen laser is used to pump a dye laser which is patterned after a laser built by Hänsch.[52] It is shown schematically in Fig. (3-3). The nitrogen laser radiation is focused on a dye cell through which flows a solution of 5×10^{-3} molar Coumarin 102 dye in ethanol. The dye laser cavity, set up at right angles to the nitrogen laser input, consists of a 2160 line/mm echelle grating which performs the dual function of end mirror and wavelength tuning element, a telescope which expands the beam size on the grating and thus enhances the grating's efficiency, and finally a fused quartz, uncoated output mirror. The dye solution lases over a wavelength interval from 4200 Å to 4700 Å with the maximum efficiency occurring at 4400 Å. The output power of the dye laser is optimized when the pulse rate is 11 pps. The dye laser is operated at a maximum average output power of 500 μwatts with a pulse duration of about 4 nsec. The linewidth of the dye laser is about 0.5 Å. Stebbings

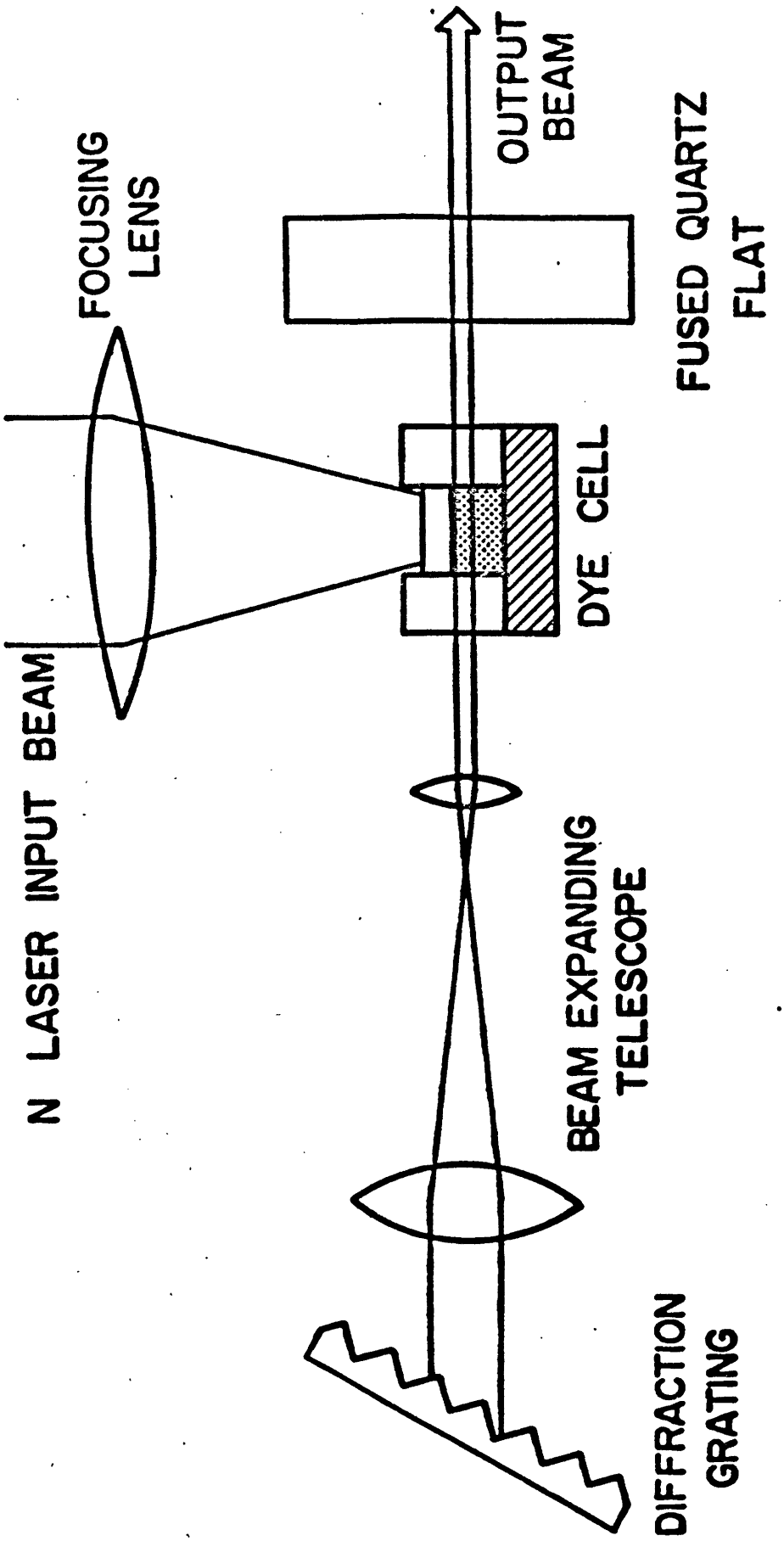

Figure (3-3) Schematic of the dye laser cavity.

et al.[44] have shown that for wavelengths (in air) decreasing from 5100 Å the laser illumination of the xenon metastables produces resonant transitions from the $^3P_0$ state to the high Rydberg states $5p^5(^2P_{3/2})np[1/2]_1$, $5p^5(^2P_{3/2})np[3/2]_1$, and $5p^5(^2P_{3/2})nf[3/2]_1$ where n starts at 11 for the p states (for a given n both np[1/2] and np [3/2] lie close together) and at 8 for the f states. The high Rydberg states excited were unambiguously identified as the ones just given by using quantum defect theory where the quantum defects for the $np[1/2]_1$, $np[3/2]_1$, and $nf[3/2]_1$ states were taken to be 3.59 ($n > 13$), 3.52 ($n > 13$), and 0.043 ($n > 11$) respectively. These transitions are shown in Fig. (3-4). The wavelength corresponding to the threshold of photoionization from the $^3P_0$ metastable state to the lower continuum is 4622 Å.

The selection rules for dipole allowed transitions in the j,ℓ coupling scheme are: $\Delta j = 0$, $\Delta k = 0, \pm 1$, $\Delta J = 0, \pm 1$, $0 \not\leftrightarrow 0$. It is seen that the above transitions correspond to $\Delta j = 1$ and therefore j,ℓ coupling is not completely adequate. Also the fact that the angular momentum of the Rydberg electron changes from $\ell = 0$ to $\ell = 3$ imples that a superposition of configurations might be a more appropriate description of the states.[44]

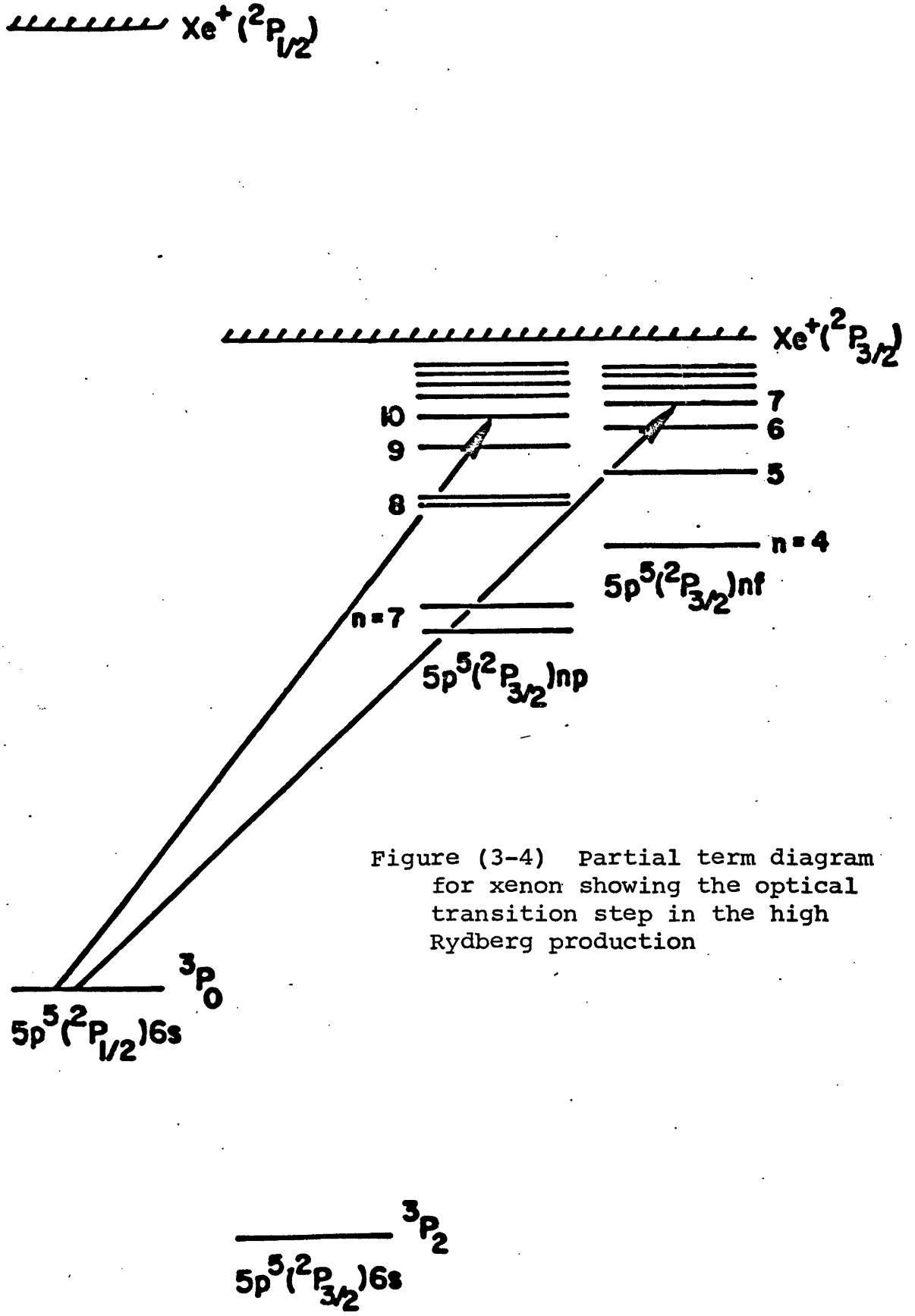

Figure (3-4) Partial term diagram for xenon showing the optical transition step in the high Rydberg production

Production of the p states having n > 16 is negligible, due it is thought[44] to configuration interaction between these states and the neighboring $5p^5(^2P_{1/2})7p'[1/2, 3/2]_1$ states in the primed series. The configuration interaction produces large intensity perturbations in the np states causing them not to be observable at high values of n. Since the f' level nearest to the nf levels excited is further away than the 7p' - np separation, such a significant intensity change is not seen in the nf high Rydberg states. Configuration interaction can also produce changes in the positions of the states with respect to energy but this effect is not detectable in the present case.[44]

The collisional ionization rate constants reported in the present work are for the individual $nf[3/2]_1$ high Rydberg states having $25 \leq n \leq 40$. The upper limit at n = 40 is determined by the laser linewidth while the lower limit at n = 25 results from the high Rydberg detection system which will be discussed later.

The laser output intersects the continuous xenon beam at right angles and each laser pulse excites a certain number of high Rydbergs. Following the pulse these excited atoms can either be allowed to collisionally ionize and the ion signal measured or they can be counted by field ionization. These processes are discussed next.

3.5 Measurement of collisional ionization signal, $S(t;Xe^+)$; Method 1.

Since it is known[45] that the presence of electric fields affects the value of the collisional ionization rate constant, it is necessary to control the residual electric fields in the interaction region. Method 1 pertains to the measurement of the collisional ionization signal in field free conditions.

Target gas is allowed to enter the chamber containing the interaction region (which therefore functions as the gas cell) through a leak valve until a total pressure in the chamber (background plus target gas) of $\sim 2 \times 10^{-6}$ torr is reached. From Fig. (3-1) it is seen that the high Rydberg atoms are actually formed inside the gas cell. This, however, does not affect the applicability of the beam-cell technique. The sequence of events in the production and collection of the collisional ions, Xe^+, occurs as follows. High Rydbergs in a selected quantum state are produced via a laser pulse intersecting the metastable Xe beam. The collision time, t_1, following the laser pulse is allowed to pass during which collisions between the Xe and the target gas occur producing Xe^+ ions. Following the time t_1 a small electric field (~40 V/cm) is applied across the interaction region and all positive ions in the region are accelerated

toward a Johnston Cu-Be particle multiplier situated at the top of the ion collector. The field is too weak to field ionize the remaining high Rydbergs in the interaction region. After the flight time, t_f, of the Xe^+ ions from the interaction region to the multiplier has elapsed the ions are detected by the multiplier and a discriminator gate of $\Delta t_1 = 1.2$ μsec duration is opened (centered about $t_1 + t_f$) to allow the counts to be registered in a scaler. During the collision time t_1 the electric field in the interaction region is maintained at ≤ 0.1 V/cm which is taken to define the meaning of "field free." The value of t_1 is variable depending on the target gas. This sequence of events is shown at the top of Fig. (3-5).

3.6 Measurement of collisional ionization signal, $S(t;Xe^+)$; Method 2.

This method is used to measure the collisional ionization signal produced in the presence of an electric field. With target gas in the cell the sequence of events for this measurement is as follows. The high Rydbergs are formed in field free conditions to ensure single state production. A short time t_2^F after the laser pulse, the electric field in which it is desired that the collisions take place is applied. Of course the magnitude of this

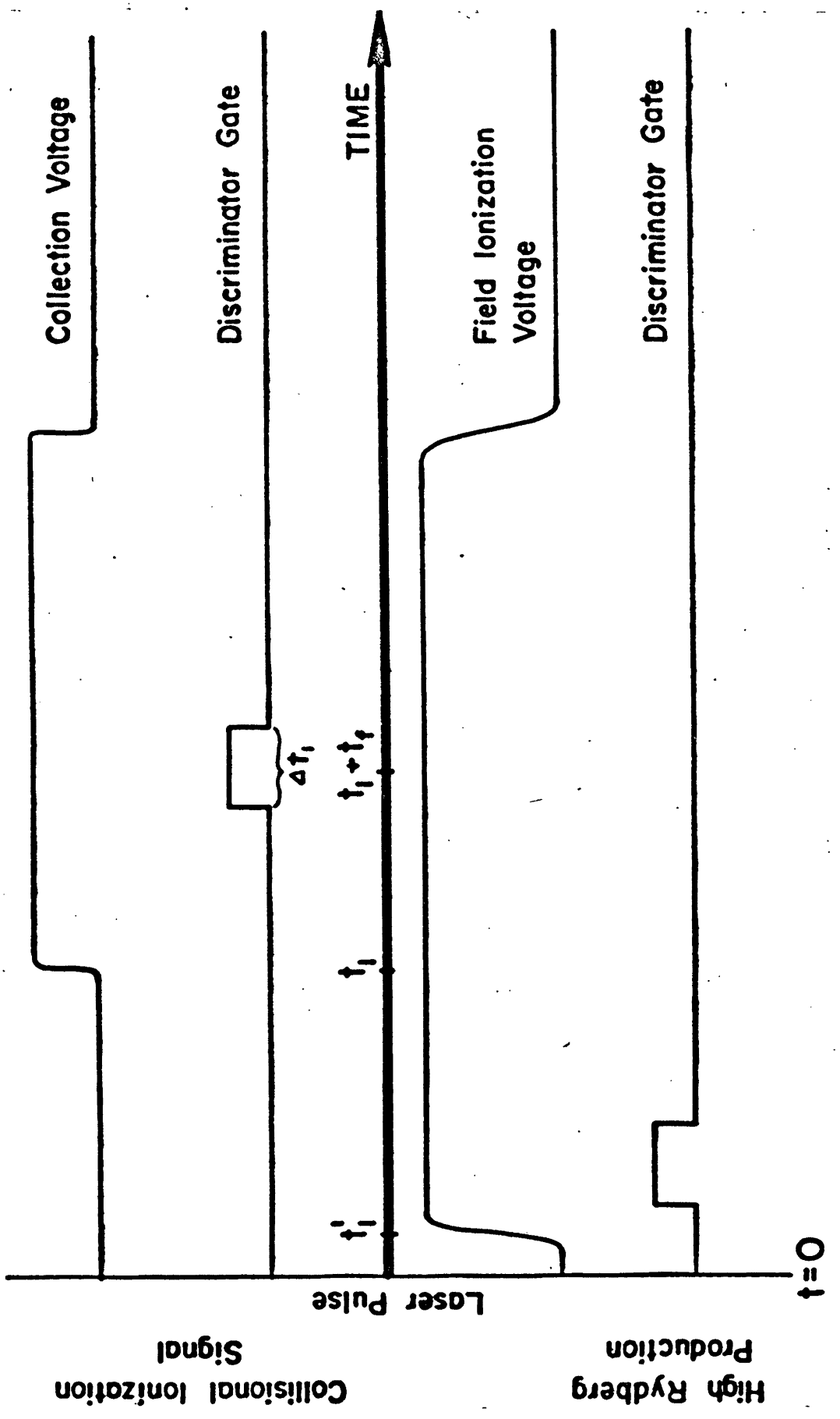

Figure (3-5) Gating sequence - Method 1

field must be less than E_c of the Rydberg state being studied. As collisions take place in this field the resulting Xe^+ ions are swept toward the particle multiplier by the field and thus there is a continuous flow of collisional ions to the multiplier. At a time t_2^G after the laser pulse ($t_2^G > t_2^F$) a discriminator gate of Δt_2 duration is opened to register counts from ions arriving at the multiplier from t_2^G to $t_2^G + \Delta t_2$. Taking into account the flight time, t_f, of the ions from the interaction region to the multiplier, the ions arriving in the discriminator gate were produced via collisions in the interaction region during the earlier time interval defined by $t_2^G - t_f$ to $(t_2^G + \Delta t_2) - t_f$. In order for the collisions producing these ions to occur in the applied field $t_f < t_2^G - t_2^F$. Since t_f is fixed once the field is chosen and t_2^F is small, this inequality actually is a limitation on the value of t_2^G. Also an "equal" sign cannot be substituted for the "less than" sign because, even though the collision interval would remain in the field, the ions formed in the time t_2^F would also be counted. This sequence of events is shown at the top of Fig. (3-6). It is seen from the foregoing discussion that the collision time interval for Method 2 is just the length of the discriminator gate, Δt_2, and, like t_1 in Method 1, it is variable

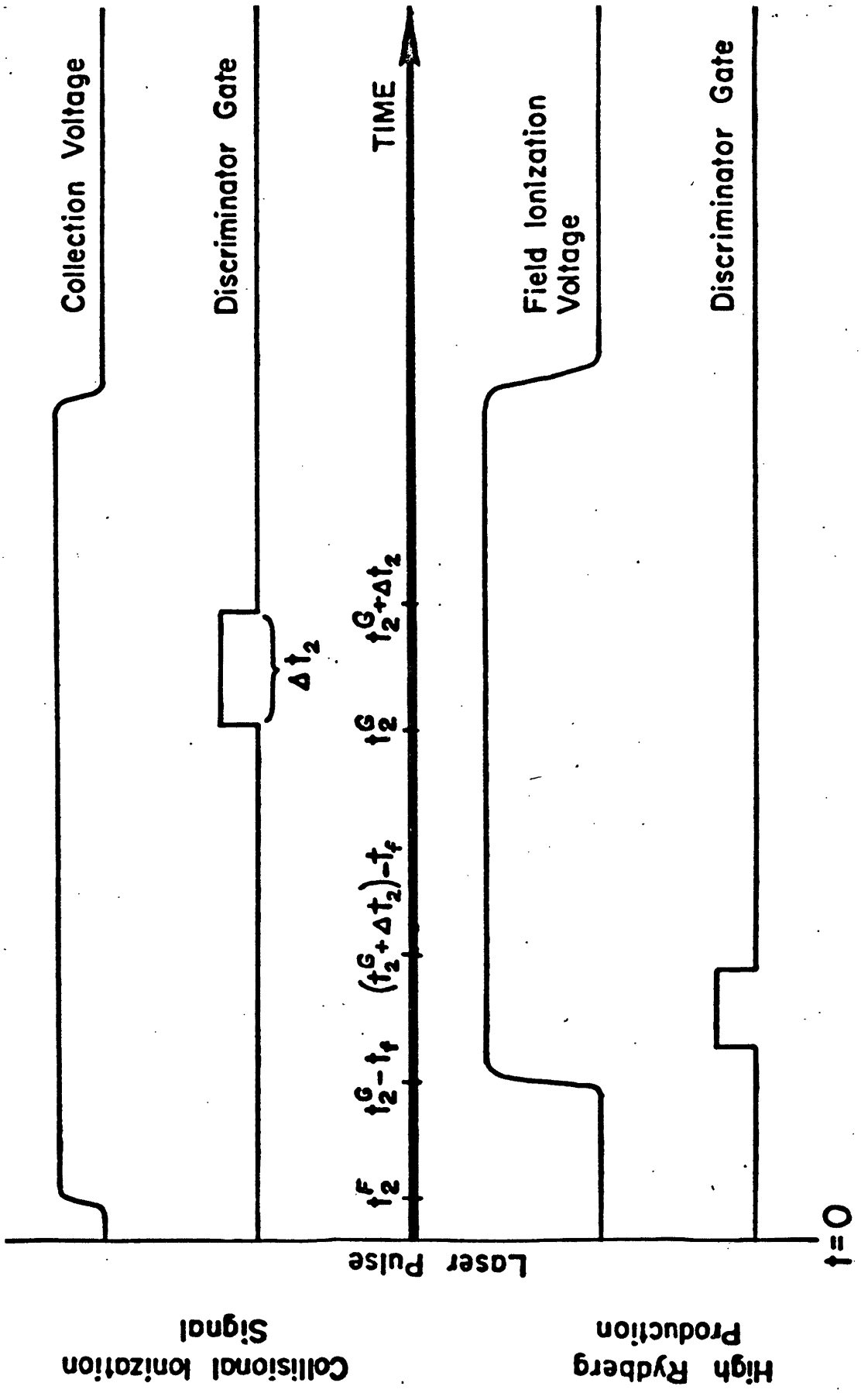

Figure (3-6) Gating sequence - Method 2

depending on the target gas. The fields employed in this method range from ~ 2 V/cm to ~ 30 V/cm.

3.7 Measurement of the number of high Rydbergs, N_o, at the start of the collision interval.

The value of N_o that is used in Eqn. (3-11) is the number of high Rydbergs that exist at the start of the collision time interval. For Method 1 this is the number of excited atoms formed in the laser pulse [$N_o = N(t = 0)$]. To measure this number an electric field exceeding the critical field of the Rydberg state is applied at a short time t_1' after the laser pulse. Application of the field after the laser pulse allows the high Rydbergs to be formed in a field free region. The field ionizes all the excited atoms present as discussed in Chapter 2 and will also sweep the ions to the multiplier in a flight time t_f. A 3 μsec discriminator gate centered about $t_1' + t_f$ registers the resultant counts in a scaler. This sequence is shown at the bottom of Fig. (3-5). The number of high Rydbergs measured by this sequence, $N(t_1')$, is the number present at time t_1', after the laser pulse and is smaller than N_o due to radiative decay of the atoms in the time interval t_1'. Therefore, to get N_o it is necessary to

extrapolate the measured number back along the exponential decay curve to the time of laser fire as follows

$$N_o = N(t_1') \, e^{t_1'/\tau} \qquad (3\text{-}12)$$

where τ is the lifetime of the Rydberg state involved.

For Method 2 the start of the collisional interval occurs at $t_2^G - t_f$ (t_f is the flight time in the small electric field in which the collision process is being studied) and consequently the ionizing field is applied at the time $t_2^G - t_f$ after the laser pulse. After allowing for the flight time of the ions in the ionizing field, a 3.0 μsec discriminator gate permits counting of these ions. There is no extrapolation necessary in this case since $N_o = N(t_2^G - t_f)$. This sequence is shown at the bottom of Fig. (3-6). It is seen that the high Rydbergs being counted are formed under field free conditions as usual.

The values of the critical fields for xenon high Rydbergs were obtained from a curve fit to the critical field data of Stebbings et al.[44] The selectivity of the field ionization process with respect to n affords a convenient technique to determine what Rydberg state the laser is producing. For a given n state application of a field less than the critical field for that n should yield no field ion signal while application of a field just

greater than the critical field should give a large field ion signal. If the state is well defined, using a field much larger than the critical field will give a signal equal to the one obtained with the $\gtrsim E_c$ field. This method of identifying Rydberg states is actually used in the present work because the wavelength setting of the spectrometer used to measure the dye laser wavelength is not exactly reproducible. The largest field that can currently be applied to the interaction region by the high voltage electronics corresponds to the critical field of n = 24. Therefore the lowest Rydberg state that can, at present, be identified by field ionization is the 25f state. This state is the lowest state studied in the present work.

3.8 Absolute rate constants.

Although a field exceeding the critical field of a given high Rydberg will ionize all such atoms, this in itself does not ensure that they will all be counted. It is necessary to take into account the detection efficiency of the particle multiplier, and unless this efficiency is unity, the number of high Rydbergs cannot be counted absolutely. The same situation exists for the detection of collisional ions. However, if the detection efficiency, k, for Xe^+ ions collected under conditions of field

ionization of the high Rydbergs equals the detection efficiency, k', for Xe^+ ions collected under collisional ionization conditions, then the efficiencies will cancel in Eqn. (3-11) since $S(t;Xe^+)$ is in the numerator while N_o is in the denominator. Thus if the ratio k/k' equals one the rate constant determined will be absolute. This ratio is measured in the present work by a photoionization technique. The laser is tuned to the $^3P_2$ to $5p^5(^2P_{1/2})$ $6p'[3/2]_1$ transition and focused to a tight spot. This is a strong transition and it is possible for a second photon in the pulse to photoionize the $6p'[3/2]_1$ state. This source of Xe^+ ions can be detected under field ionization or collisional ionization conditions and the ratio of the two measured signals determined. This ratio equals the ratio of the detection efficiencies. The ratio has been shown to be equal to one to within 5%. Thus the rate constants measured in the present work are absolute.

3.9 Measurement of target gas pressure.

The value of the target gas pressure needs to be known more accurately than the approximate value given earlier. This pressure is measured on an ionization gauge and because the response of such a gauge changes for different gases, it must be calibrated for each target gas

used. This calibration is accomplished with an MKS Baratron Pressure Meter which measures absolute pressures independent of the type of gas by means of a capacitance manometer. The Baratron Meter cannot be used to directly measure the target gas pressure under experimental conditions because its most accurate range is about 10^{-4} to 10^{-5} torr which is well above the target gas pressure during an experiment. Pressure readings given by both the Baratron Meter and the ionization gauge are recorded at a high target gas pressure ($\sim 5 \times 10^{-5}$ torr as measured on the ionization gauge) and at the background gas pressure (target gas pressure $\sim$ 0 torr). A calibration factor is obtained by dividing the change in pressure as measured by the Baratron Meter by the change in pressure as measured by the ionization gauge. Since the Baratron Meter measures actual pressure, the pressure as measured by the ionization gauge, when multiplied by the calibration factor gives the actual pressure (zero offsets are negligible). The calibration factors for the target gases are:

Gas	Factor
CCl_4	0.32
H_2O	1.22
NH_3	0.80

H_2S	0.71
SO_2	0.9
CCl_3F	0.38
CCl_2F_2	0.53

The uncertainty in the calibration technique itself appears to be $\leqslant 5\%$[53] while additional problems with drift in the pressure and contamination of the ionization gauge increase this value to give a total uncertainty in the target gas pressure of $\sim$ 10%.

In Eqn. (3-11) n is the number density of the target gas molecules and is given by

$$n = (P_{I.G.})(3.22 \times 10^{16})(F)$$

where $P_{I.G.}$ is the target gas pressure in torr as measured by the ionization gauge, 3.22×10^{16} is the number density per torr at room temperature, and F is the calibration factor.

3.10 Lifetimes, τ; Gating sequence times.

For the determination of rate constants under zero field conditions, the xenon high Rydberg lifetimes were obtained from a curve fit to the field free lifetime data of Stebbings *et al.*[44] For the rate constants measured as

a function of applied electric field the high Rydberg state 28f is used in all cases and the lifetimes as a function of field for this state were obtained from the non-zero field data of Stebbings et al.[44] Both field free and non-zero field lifetimes have an uncertainty of 6%.

The various sequences of voltages and discriminator gates are displayed on an oscilloscope and the measurements of all times associated with these sequences are made on the oscilloscope (2 μsec/cm time base). Flight times are measured by displaying the discriminator output on the oscilloscope and looking for the arrival time after the laser pulse of the Xe^+ ions produced either by the photo-ionization technique (see Sec. 3.8) or the actual experimental signal under the appropriate electric field configuration. All measured times have an uncertainty of 5%.

3.11 Experimental details.

In order to be able to use Eqn. (3-11) it is necessary to ensure that thin target conditions prevail in the interaction region. If such conditions do not exist the measured rate constants will be too small. In the present experiment the target is said to be "thin" if the collisional ionization signal is $\leqslant$ 10% of the high Rydberg production.

In gathering sufficient data to be able to determine a cross section the measurement of high Rydberg production is alternated with the measurement of collisional ionization signal. In order to reduce the data acquisition time, target gas is left in the interaction region during the high Rydberg production measurement even though the measurement can be made with the gas removed. For the counting periods employed in this experiment, the nominal uncertainty due to the statistical counting process is 7%.

In both of the gating sequences used to measure the high Rydberg production, $N(t_1')$ and $N(t_2^G - t_f)$, and in Method 1 of the collisional ionization measurement, $S(t_1;Xe^+)$, fields are applied which sweep all the positive ions that have accumulated in the interaction region to the particle multiplier in a group. For any ions that impact simultaneously on the multiplier only one count will be registered. Therefore it is necessary to reduce the number of ions reaching the multiplier on the average to less than one per laser pulse. This is accomplished by inserting neutral density filters into the laser beam by various known amounts. In practice the attenuation required during the Method 1 collisional ionization measurement, $S(t_1;Xe^+)$, is small or zero due to the low signal levels. In Method 2 of the collisional ionization measurement,

$S(\Delta t_2;Xe^+)$, the possibility of simultaneous Xe^+ ion arrival at the multiplier is reduced because the ions are swept to the multiplier as they are formed and do not accumulate in the interaction region. In counting the high Rydbergs formed, the laser beam is usually attenuated by a factor of ten. Since the laser beam intensity is decreased more for high Rydberg production counting than for collisional ion counting, the number of high Rydbergs that is measured must be multiplied by a net attenuation factor which accounts for the difference in the neutral density filters used in the two counting modes. This procedure is correct only if the number of high Rydbergs, formed when the smaller neutral density filter is in the laser beam, is equal to the number obtained by multiplying, by the attenuation factor, the measurement taken when the larger filter is in the beam. This is true for average laser powers of less than 500 μwatts, with the present apparatus. The uncertainty in the amount of attenuation for any neutral density filter is 8%.

Since counting processes are statistical in nature, it is possible even with appropriate attenuation for two ions to arrive at the multiplier simultaneously for any of the gating sequences. Consequently, it is necessary to correct the measured signal for this possibility. The

dead time correction factor used in this work has been derived by West.[51]

The gating sequences (either Method 1 or 2) used to measure the number of high Rydbergs formed and the collisional ionization signal, ideally would count only Xe^+ ions formed via field ionization of high Rydbergs or collisions between the high Rydbergs and the target gas. In practice, in addition to the Xe^+ ions just mentioned, positive ions due to a variety of other processes are also counted. Since N_o and $S(t;Xe^+)$ are allowed to contain only Xe^+ ions produced by high Rydberg field ionization and by collisional ionization of the high Rydbergs by the target gas, this spurious signal, while not large in the present experiment, cannot be neglected. It can arise, in the case of the $N(t_1')$ and $N(t_2^G - t_f)$ measurements, from chemiionization of certain background and target gases by the xenon metastables, from chemiionization of certain background and target gases by the high Rydbergs in the time t_1' or $t_2^G - t_f$, from the collisional ionization of the high Rydbergs by the background and target gases in the time t_1' or $t_2^G - t_f$, and from photoionization of the background, target, and xenon gases by the laser. The background and target gas chemiions formed by xenon metastables are counted independently

of the rest by following the same gating sequence as in the measurement of $N(t_1')$ or $N(t_2^G - t_f)$ except that the laser beam is excluded from the interaction region. This measurement is then subtracted from the result obtained when the laser beam is not excluded. Penning ionization of the target gas by high Rydbergs is not possible for H_2O, SO_2, or CCl_2F_2 since the ionization potentials of these target gases are greater than 12.1 eV. For targets with ionization potentials below 12.1 eV and whose masses are appreciably different from Xe, any Penning ions produced should not be counted in the discriminator gate due to the difference in flight time between these ions and Xe^+. Penning ions whose masses are comparable to Xe will not be excluded in this manner. To examine the possibility of CCl_4^+ production a time of flight experiment was conducted which would separate CCl_4^+ ions from Xe^+ ions. In this experiment a spectrum of the time of flight from the interaction region to the multiplier of Xe^+ ions produced by the photoionization method (see Sec. 3.8) is obtained. This is compared with the time of flight spectrum of Xe^+ and CCl_4^+ (if any) ions formed in collisional ionization. Due to the difference in the mass of these two ions, the second spectrum should be broader with respect to time than the Xe^+ spectrum. The minimum broadening detectable is ~ 1 μsec. To the accuracy of the method no CCl_4^+

was observed. Penning ionization of the background gas by the high Rydbergs cannot be ruled out. Also associative and rearrangement ionization of both the background and target gases by the high Rydbergs may occur. Such interactions have been argued to be small by West[51]; Hotop and Niehaus[17] have estimated the cross section for

$$Ar^{**} + H_2 \rightarrow ArH^+ + H + e$$

where Ar** is a high Rydberg argon atom, to be $\sim 10^{-14}$ cm^2. In addition another time of flight experiment was carried out in the present work which would distinguish XeH_2O^+ from Xe^+ when H_2O is the target gas. To the accuracy of the method XeH_2O^+ was not detected. The amount of collisional ionization of the high Rydbergs by the target gas that occurred in the time t_1' or $t_2^G - t_f$ can be estimated by using Eqn. (3-11) where the collision time t is now t_1' or $t_2^G - t_f$ and by using the rate constant obtained if this particular process is ignored. (This is a satisfactory estimate because the number of collisional ions is small and therefore only a first order value of that number is needed.) The number of collisional ions so obtained is then subtracted from the value of $N(t_1')$ or $N(t_2^G - t_f)$ measured as in section 3.7. Finally, single step photoionization by the laser is not energetically

possible for xenon or any of the target gases. Although the composition of the background gas is unknown such photoionization is unlikely for it as well. Multiple step photoionization is possible for any of the gases but is again unlikely due to the fact that the laser beam is not strongly focused. Also photoionization cross sections are generally small. These conclusions support the findings of West[51] who failed to detect such ions formed under the present experimental conditions.

In the case of the collisional ionization signal measurements, $S(t_1;Xe^+)$ or $S(\Delta t_2;Xe^+)$, chemiionization of the background and target gases by the xenon metastables and high Rydbergs, collisional ionization of the high Rydbergs by the background gas, and photoionization of the background, target, and xenon gases by the laser are responsible for the spurious ions counted. By following the same gating sequence as for the measurement of $S(t_1;Xe^+)$ or $S(\Delta t_2;Xe^+)$ except with the target gas removed, the chemiionization of the background gas by the xenon metastables and high Rydbergs, the collisional ionization of the high Rydbergs by the background gas, and photo-ionization (although small for reasons given above) can be determined and accounted for. Penning ionization of the target gas by xenon metastables is not possible for any of

the target gases since the ionization potentials of these gases are greater than 9.45 eV. The chemiionization of the target gas by the high Rydbergs can be dismissed for reasons given in the last paragraph, above.

In method 1 of the collisional ionization measurement the collision time was stated above to be t_1. This is only strictly true if the discriminator gate has zero width in time and if all collisional ions are registered instantaneously at $t_1 + t_f$. However, in practice, the Xe^+ ions have a finite spread in their flight time spectrum which necessitates the use of a finite gate width to ensure total collection. This gate is 1.2 μsec wide and is centered about $t_1 + t_f$ where t_f is the mean flight time. Consequently, it is possible to detect some ions in the last part of the gate ($\sim$ 0.6 μsec) that are formed after the field is applied. In order to account for this ion production the collision time that is actually used in Eqn. (3-11) is t_1 plus that part of the gate which follows the mean arrival time of the ions, $t_1 + t_f$.

A possibility exists that the high Rydbergs produced can have their quantum state altered due to collisions.[40] This would result in high Rydbergs which are no longer well defined. However, for the experimental conditions employed in this laboratory, West[51] and West et al.[45]

have argued against such an occurrence.

Finally, the absolute rms uncertainty in the present collisional rate constant measurements is $\pm$ 20% while the relative rms uncertainty is $\pm$ 15%.

CHAPTER 4

Results and Discussion

4.1 Overall results.

The values of the absolute rate constants measured in field free conditions for the various high Rydberg states and target gases studied are given in Tables (4-1) to (4-7). The value of ℓ of the high Rydberg states having $n \geq 35$ is not determined but is probably f.[44] The uncertainties given for the value of $n \geq 35$ result from difficulties encountered in populating just one state. In Figs. (4-1) through (4-5) these rate constants are plotted as a function of the principal quantum number of the Rydberg electron. The behavior of the rate constants measured in the presence of an electric field is displayed in Figs. (4-6) through (4-10) for the particular gases so investigated (CCl_4, H_2O, NH_3, H_2S, and CCl_3F). In this chapter these results will be compared with other experimental work and with theory. Before this comparison is made, however, a discussion of the nature of the rate constants measured in this work will be undertaken and cross sections corresponding to the rate constants will be derived.

Table 4-1

Results for CCl_4

State	k_c (10^{-7} cm^3/sec)	σ_c (10^{-12} cm^2)	Binding energy of Rydberg electron (meV)
Xe(25f)	2.9	9.1	21.8
Xe(28f)	2.4	7.5	17.4
Xe(29f)	2.6	8.1	16.2
Xe(33f)	3.4	10.5	12.5
Xe[(37$\pm$1)f]	3.8	11.8	9.96
Xe[(40$\pm$2)f]	4.2	13.1	8.52

Table 4-2

Results for H_2O

	State	k_c (10^{-7} cm^3/sec)	σ_c (10^{-12} cm^2)
Present results	Xe(25f)	2.3	1.6
	Xe(27f)	4.1	2.8
	Xe(30f)	5.1	3.5
	Xe(32f)	5.9	4.1
	Xe[(35±1)f]	7.7	5.4
	Xe[(37±1)f]	10.5	7.3
	Xe[(40±2)f]	14.5	10.1
Hotop and Niehaus[16]	He**		0.29 ± 0.05
	Ne**		0.78 ± 0.06
	Ar**		1.2 ± 0.08

Table 4-3

Results for NH_3

	State	k_c (10^{-7} cm^3/sec)	σ_c (10^{-12} cm^2)
Present results	Xe(25f)	0.80	0.53
	Xe(28f)	2.0	1.4
	Xe(31f)	2.9	1.9
	Xe(32f)	3.2	2.2
	Xe[(36±1)f]	4.4	3.0
	Xe[(40±2)f]	5.5	3.7
Hotop and Niehaus[16]	He**		0.15 ± 0.04
	Ar**		0.74 ± 0.07

Table 4-4

Results for H_2S

	State	k_c (10^{-7} cm^3/sec)	σ_c (10^{-12} cm^2)
Present results	Xe(25f)	0.41	0.49
	Xe(27f)	0.56	0.67
	Xe(29f)	0.81	0.96
	Xe(33f)	1.3	1.6
	Xe[(37$\pm$1)f]	2.4	2.9
	Xe[(39$\pm$2)f]	2.4	2.8

Table 4-5

Results for SO_2

	State	k_c (10^{-8} cm^3/sec)	σ_c (10^{-13} cm^2)
Present results	Xe(32f)	1.8	3.5
	Xe[(36±1)f]	3.4	6.5
	Xe[(37±1)f]	4.8	9.2
	Xe[(40±2)f]	6.8	12.9
Hotop and Niehaus[16]	He**		1.1 ± 0.5
	Ne**		2.7 ± 0.7
	Ar**		4.0 ± 0.9

Table 4-6

Results for CCl_3F

State	k_c (10^{-7} cm^3/sec)	σ_c (10^{-11} cm^2)	Binding energy of Rydberg electron (meV)
Xe(25f)	3.6	1.1	21.8
Xe(27f)	4.4	1.3	18.7
Xe(28f)	4.2	1.2	17.4
Xe(29f)	4.5	1.3	16.2
Xe(33f)	5.8	1.7	12.5
Xe[(37±1)f]	5.6	1.7	9.96
Xe[(40±2)f]	6.2	1.9	8.52

Table 4-7

Results for CCl_2F_2

State	k_c (10^{-8} cm^3/sec)	σ_c (10^{-13} cm^2)	Binding energy of Rydberg electron (meV)
Xe(27f)	1.9	5.3	18.7
Xe(31f)	1.6	4.4	14.2
Xe(33f)	1.5	4.1	12.5
Xe[(37±1)f]	0.80	2.2	9.96
Xe[(40±2)f]	0.97	2.7	8.52

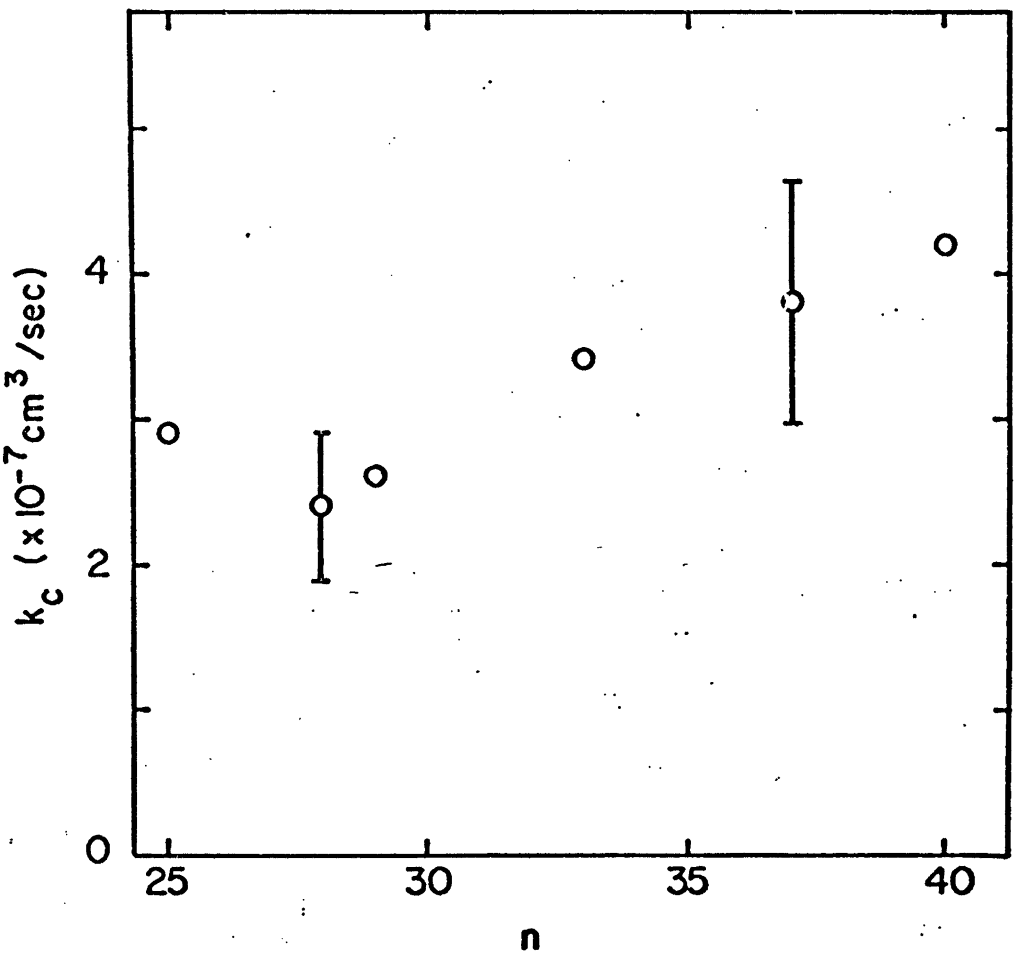

Figure (4-1) Results for the reaction

$Xe(nf) + CCl_4 \rightarrow Xe^+ + (CCl_4 + e)$.

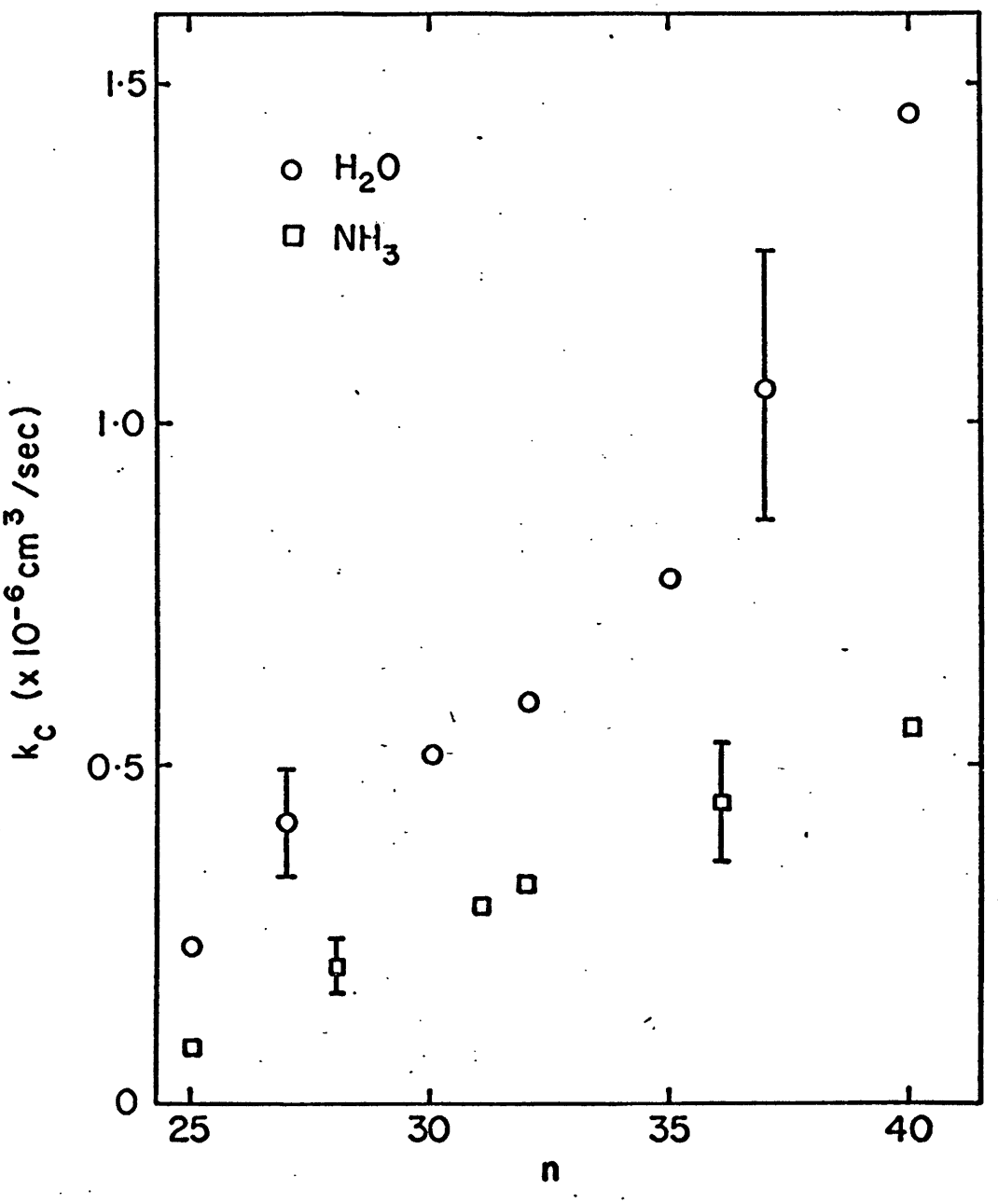

Figure (4-2) Results for the reactions

$$Xe(nf) + H_2O \rightarrow Xe^+ + H_2O + e$$

$$Xe(nf) + NH_3 \rightarrow Xe^+ + NH_3 + e\,.$$

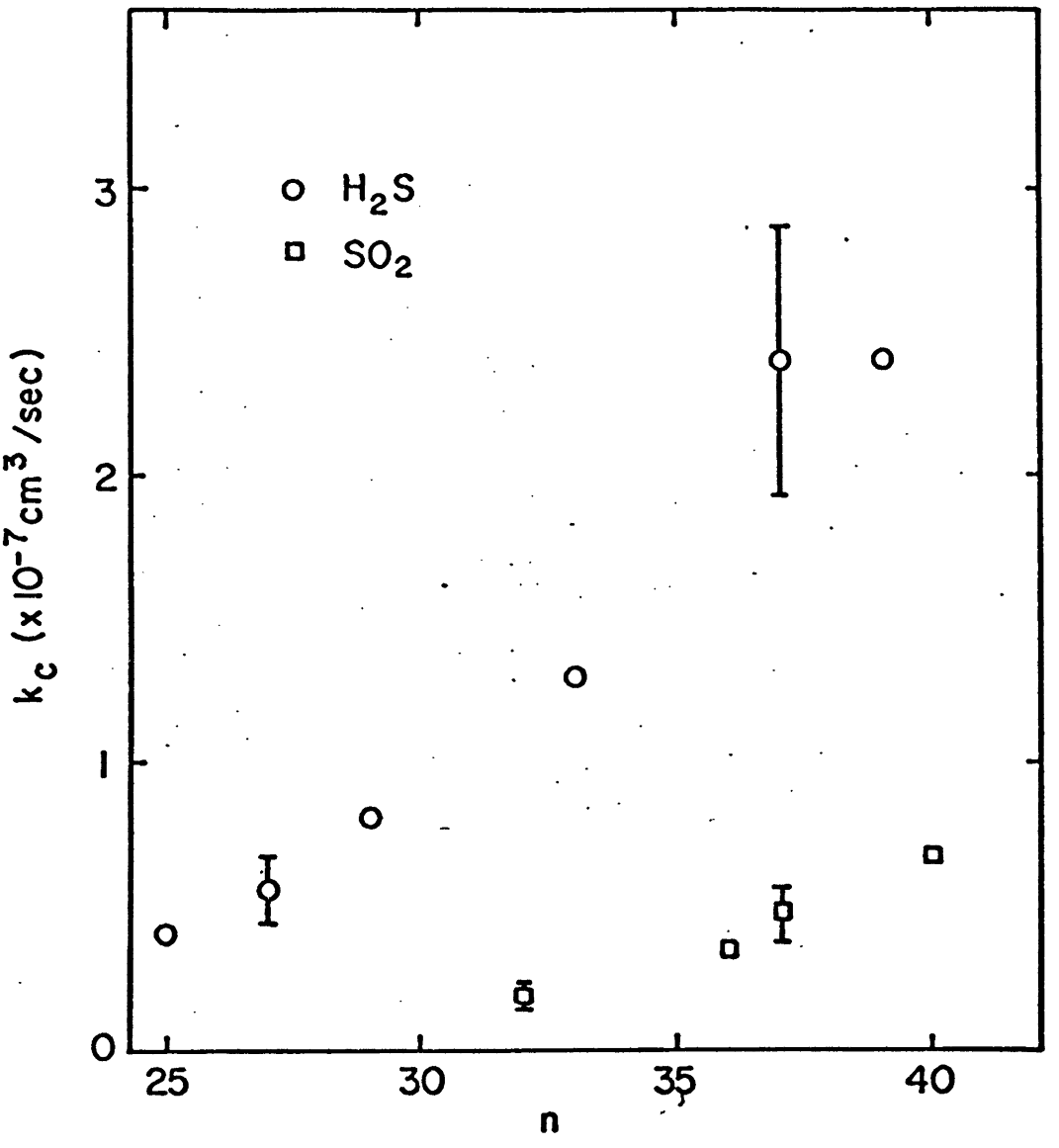

Figure (4-3) Results for the reactions

$$Xe(nf) + H_2S \rightarrow Xe^+ + H_2S + e$$

$$Xe(nf) + SO_2 \rightarrow Xe^+ + SO_2 + e$$

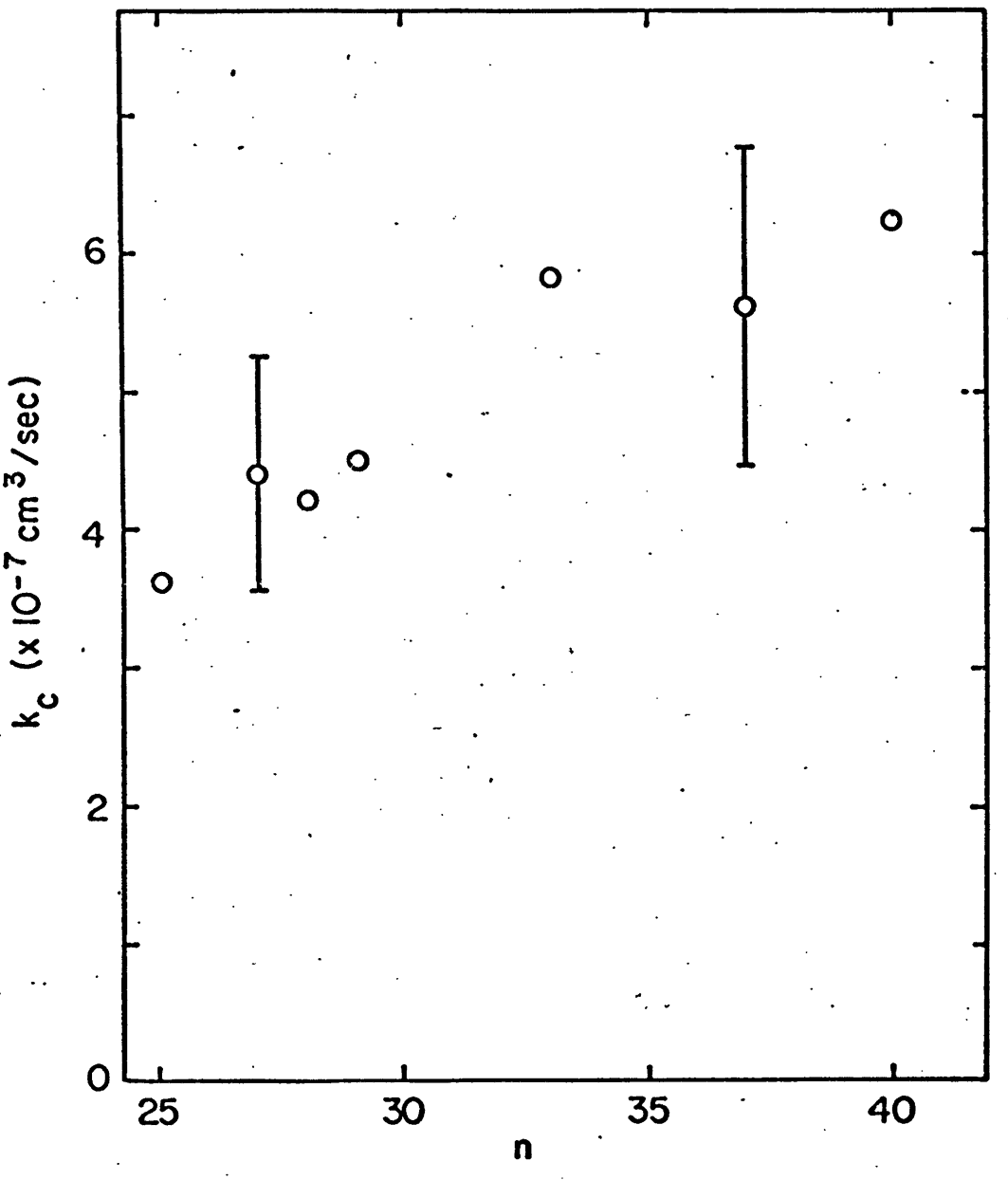

Figure (4-4) Results for the reaction

$Xe(nf) + CCl_3F \rightarrow Xe^+ + (CCl_3F + e)$.

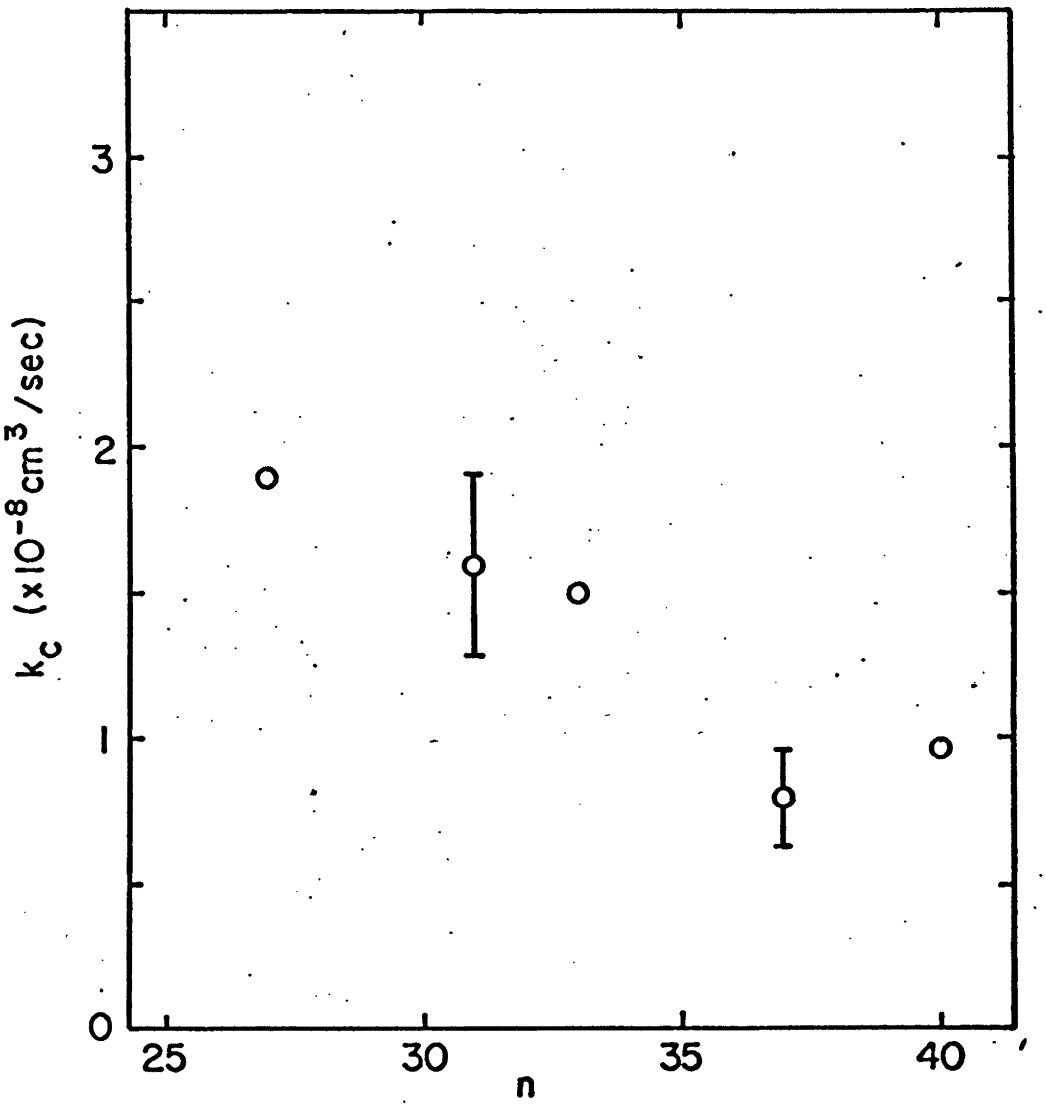

Figure (4-5) Results for the reaction

$$Xe(nf) + CCl_2F_2 \rightarrow Xe^+ + CCl_2F_2 + e.$$

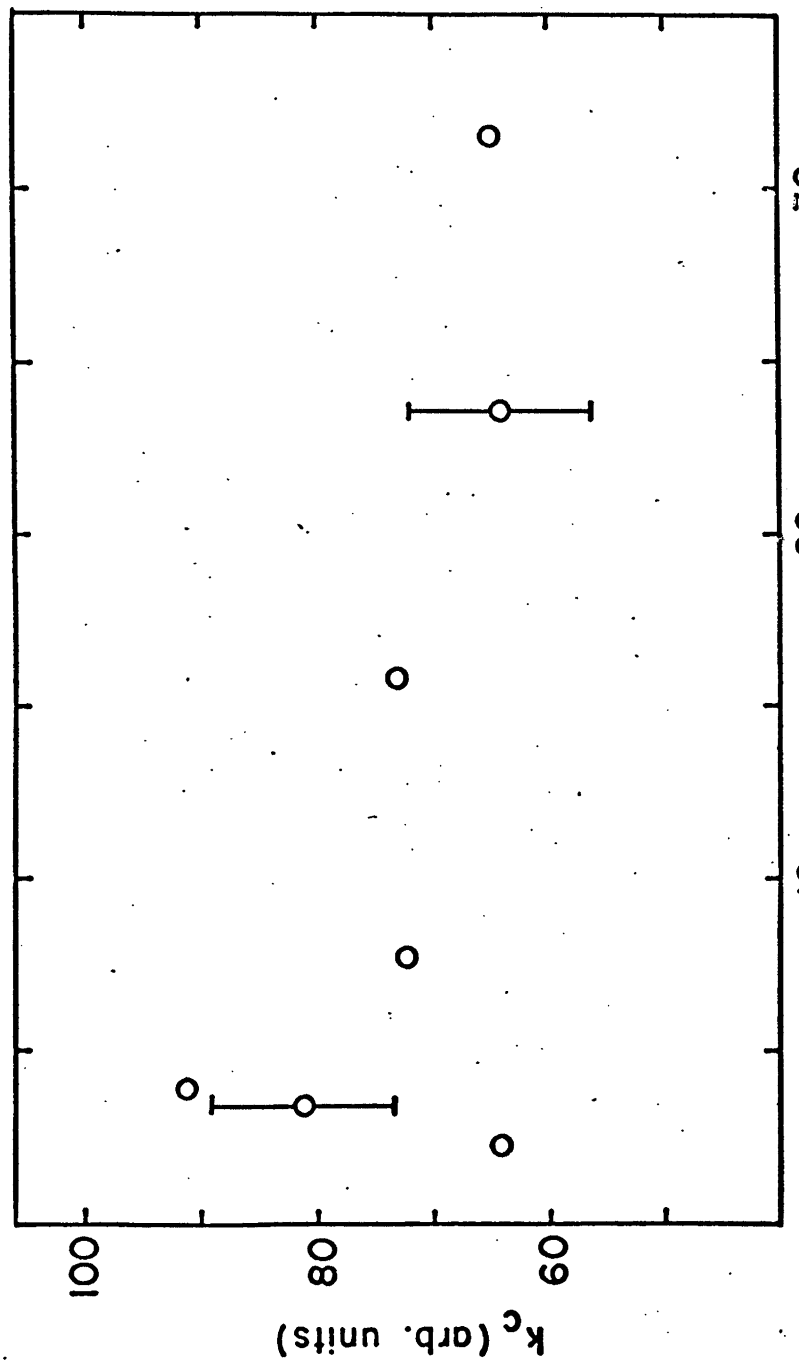

Figure (4-6) Results for the reaction Xe(nf) + CCl_4 → Xe^+ + (CCl_4 + e) in an applied electric field.

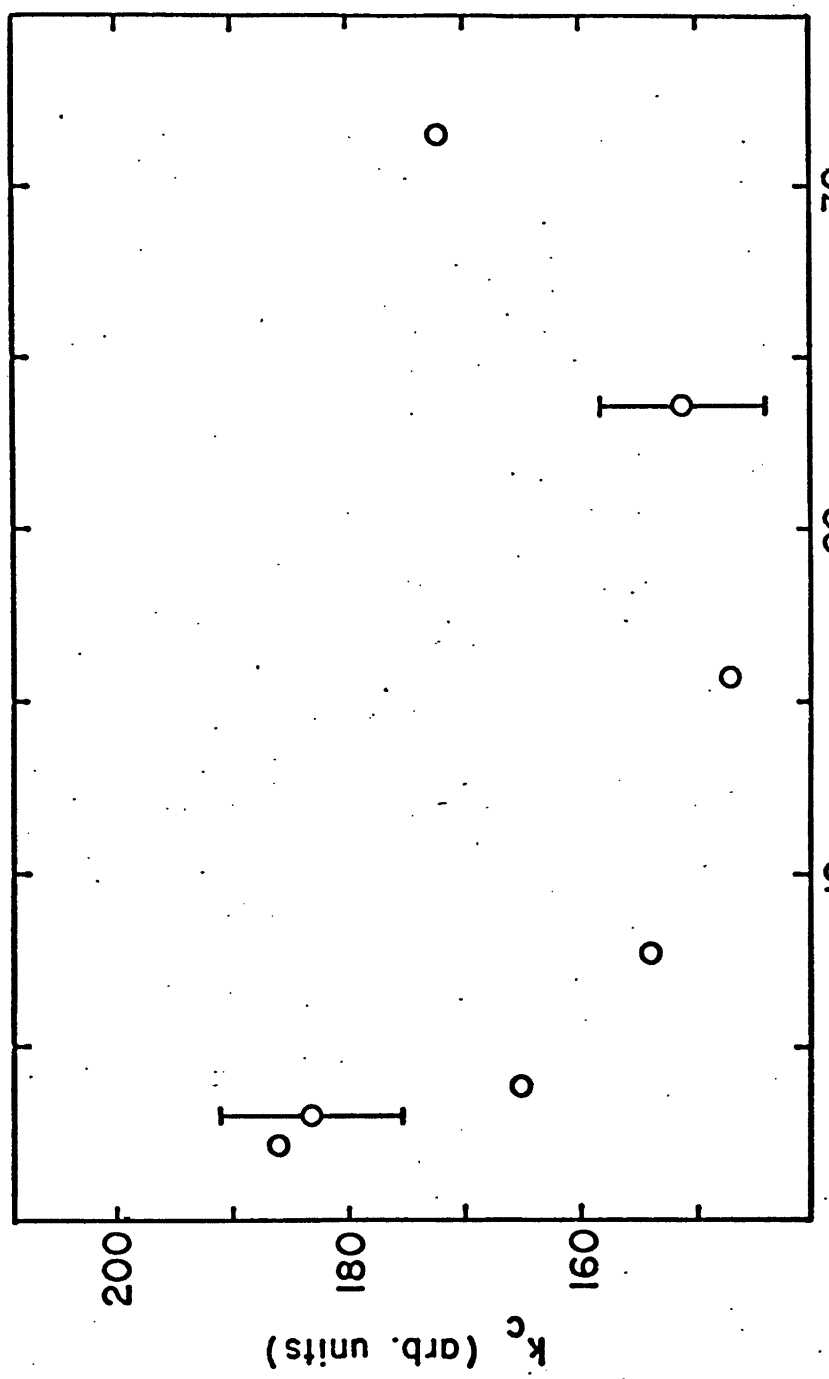

Figure (4-7) Results for the reaction $Xe(nf) + H_2O \rightarrow Xe^+ + H_2O + e$ in an applied electric field.

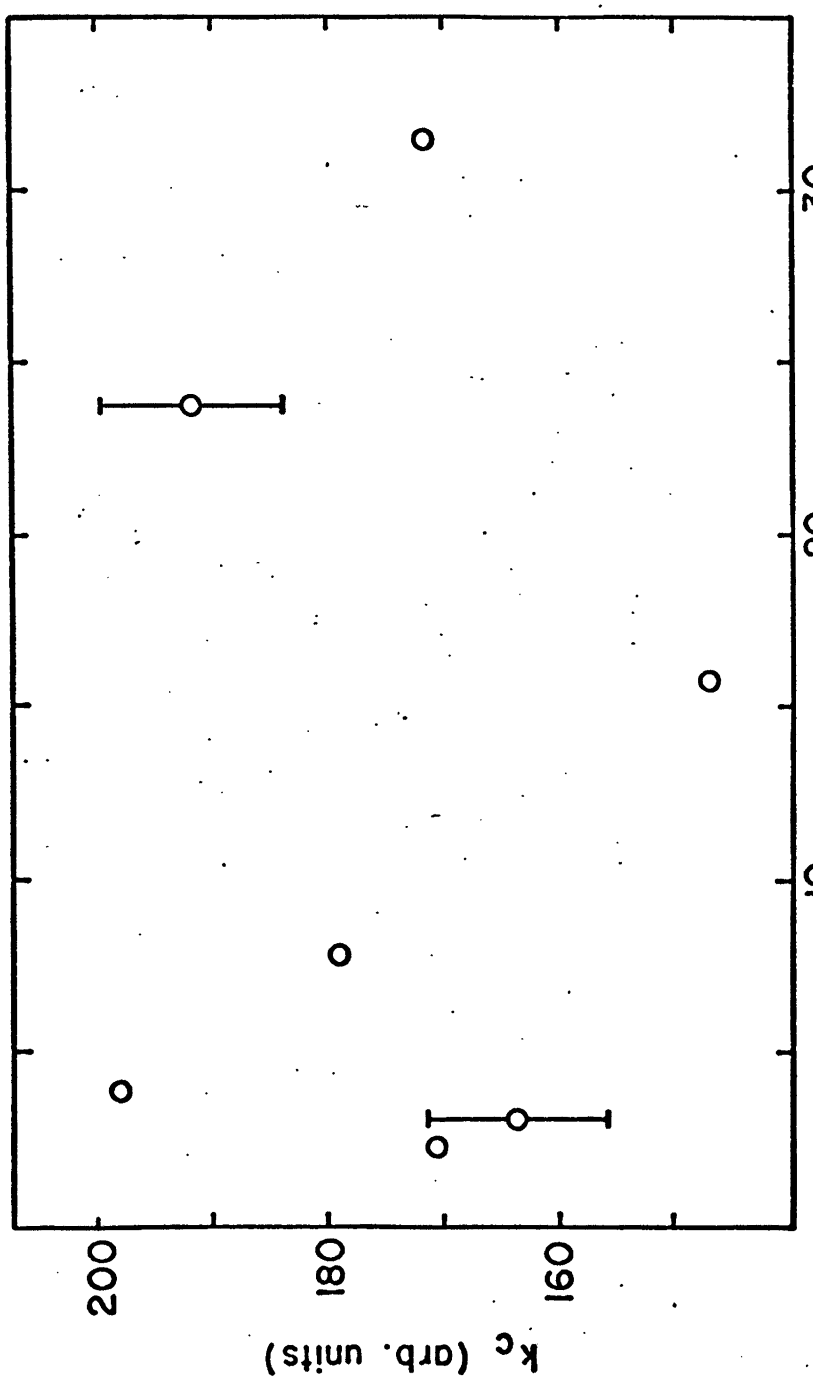

Figure (4-8) Results for the reaction $Xe(nf) + NH_3 \rightarrow Xe^+ + NH_3 + e$ in an applied electric field.

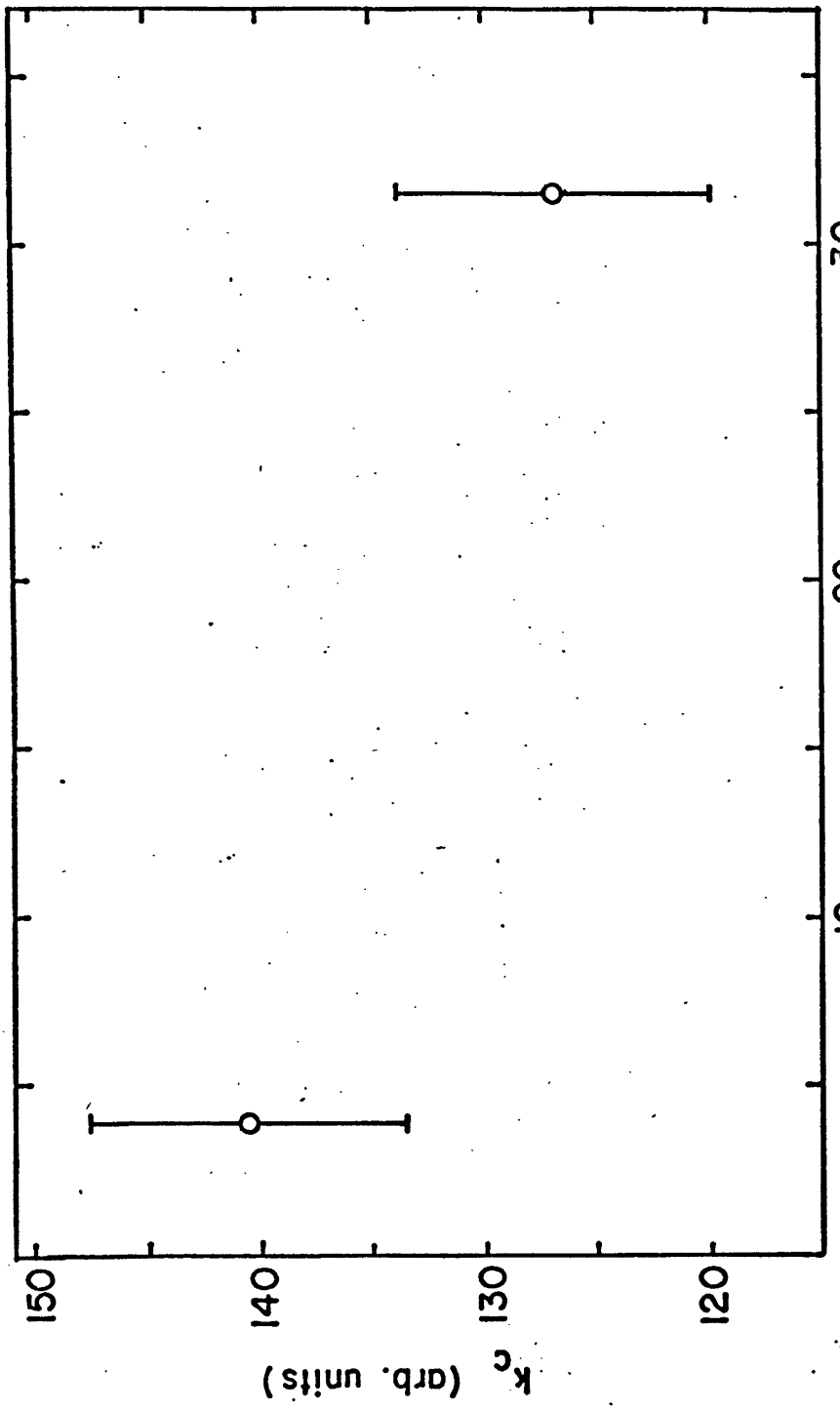

Figure (4-9) Results for the reaction $Xe(nf) + H_2S \rightarrow Xe^+ + H_2S + e$ in an applied electric field.

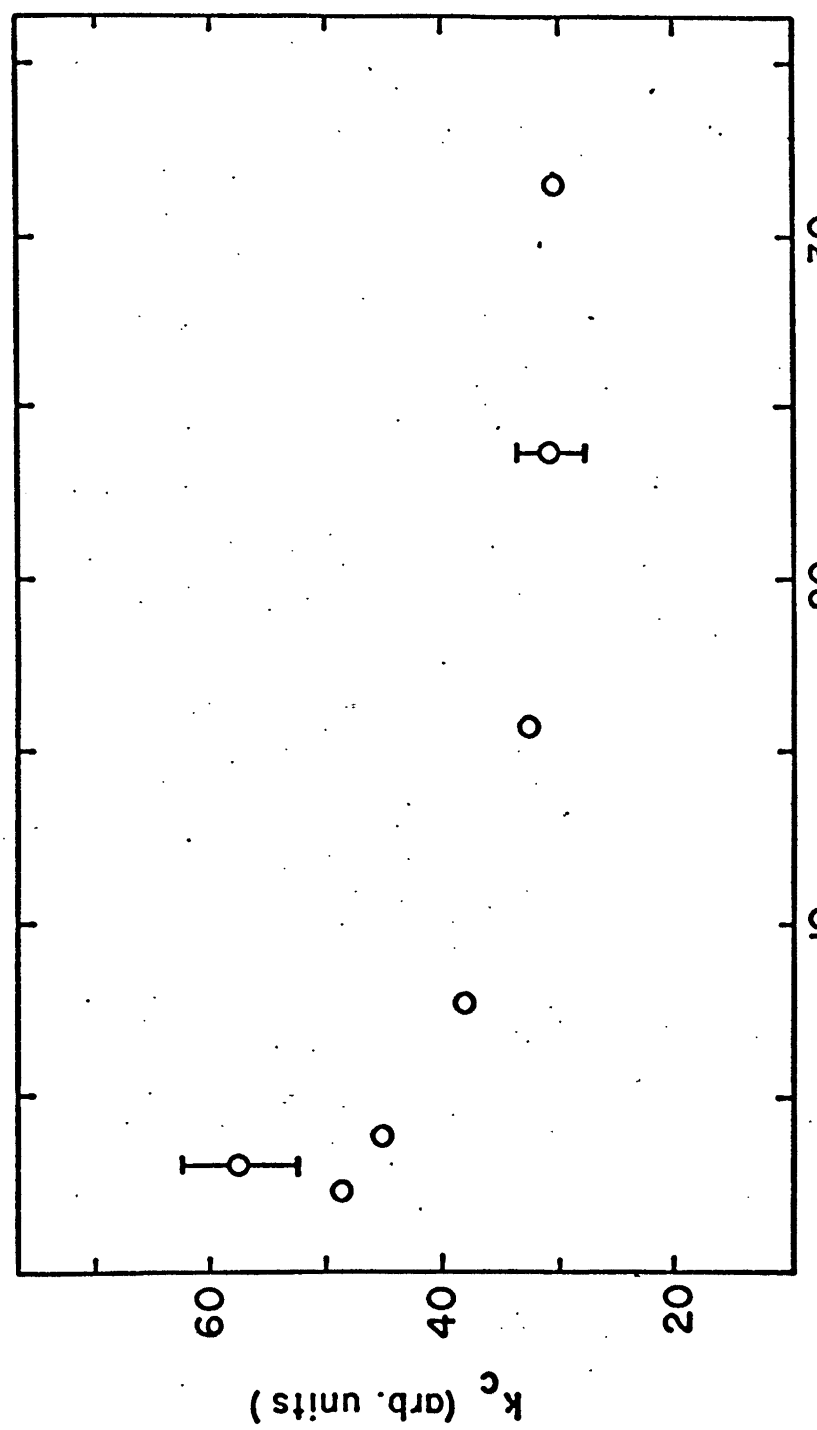

Figure (4-10) Results for the reaction Xe(nf) + $CCl_3F \rightarrow Xe^+ + (CCl_3F + e)$ in an applied electric field.

4.2 Discussion of the rate constant as it is measured in this work and the calculation of cross sections.

For the process of collisional ionization of a high Rydberg, A**, by a molecule BC

$$A^{**} + BC \rightarrow A^{+} + (BC + e) \qquad (4\text{-}1)$$

a rate constant, k_c, can be defined in the traditional manner by the rate equation

$$\frac{d[A^{**}]}{dt} = -k_c[A^{**}][BC] \qquad (4\text{-}2)$$

where the square brackets denote number densities of the species they contain. It is necessary to exercise a little caution in the use of rate equations like Eqn. (4-2). The reason for this is that the value of the rate constant depends on the relative velocity distribution between the two reactants -- a fact which is not apparent from the rate equation. This means that in order for the results obtained from the rate equation to be correct the conditions under which a reaction takes place must be the same as the conditions under which the rate constant has been measured or derived. For instance, rate equations are normally applied to situations in which the reactants each possess a Maxwellian velocity distribution. Consequently, the rate constant used in the equation must

be one that has been determined for these same Maxwellian velocity distributions. A different situation exists in the present experiment. The high Rydbergs comprise a beam which has a certain (non-Maxwellian) velocity distribution expressed as[54]

$$\mathcal{F}(v_1) = \frac{m_1}{kT} v_1 \exp(-m_1 v_1^2/2kT) \qquad (4\text{-}3)$$

where v_1 and m_1 are the speed and mass of the xenon atom respectively and T equals 300° K. The distribution is only one dimensional because the motion in the beam is only in one dimension. The target gas confined in the gas cell obeys the Maxwellian velocity distribution

$$\mathcal{F}(\vec{v}_2) = \left(\frac{m_2}{2\pi kT}\right)^{3/2} \exp(-m_2 v_2^2/2kT) \qquad (4\text{-}4)$$

where $\vec{v}_2$ and m_2 are the velocity and mass of the target molecule respectively and T equals 300° K. Thus the rate constant, k_c, measured in the present experiment is appropriate to Eqn. (4-1) only when the reaction occurs with the velocity distributions given by Eqns. (4-3) and (4-4) and the application of Eqn. (4-2) to the reaction using this k_c will only give correct results for the beam-cell geometry. In fact, Eqn. (4-2) can be integrated under the assumption of a beam-cell geometry, to give

Eqn. (3-11), the expression used in this experiment to determine k_c, if t_{eff} is used and the additional assumption concerning thin target conditions is also made. (This last assumption about the target condition does not place any limitations on the applicability of the measured k_c to different situations; such conditions are employed to simplify the experimental work.)

The conclusion to be drawn from the above discussion is that the specification of a rate constant for a given reaction is not the best description of that reaction. Rather, a description in terms of the more fundamental property, the cross section, is more appropriate. The relationship between a rate constant and the cross section is given by Eqns. (3-4) and (3-5) where the explicit dependence of the rate constant upon the velocity distributions of the reactants is apparent. Given the cross section of a reaction as a function of the relative velocity of the reactants, a rate constant appropriate to any combination of reactant velocity distributions can be obtained.

Since the cross section of a reaction is the more appropriate quantity to know, approximate cross sections to which the rate constants in the present work correspond are obtained by removing σ from under the integrals in

Eqn. (3-4) and thereby giving the familiar result

$$k = \sigma \bar{v}_r \tag{4-5}$$

where

$$\bar{v}_r = \iint v_r \mathcal{F}(\vec{v}_1) \mathcal{F}(\vec{v}_2) \, d^3v_1 \, d^3v_2 \tag{4-6}$$

and is just the average relative speed between the reactants. The cross sections calculated in this manner are quite accurate if σ varies slowly with v_r over the range of v_r where the velocity distributions are appreciable. If σ is actually independent of v_r or if the velocity distributions are Dirac delta functions of their arguements (i.e., monoenergetic beam on a stationary target), then σ obtained from Eqns. (4-5) and (4-6) is exact. In the present case of a beam-cell geometry $\mathcal{F}(\vec{v}_1)$ is given by Eqn. (4-3) while $\mathcal{F}(\vec{v}_2)$ is given by Eqn. (4-4). For these distributions the above integral has been evaluated in closed form by West[51] with the result being

$$\bar{v}_r = \left(\frac{\pi kT}{2}\right)^{1/2} m_1^{1/2} \left(\frac{1}{m_1} + \frac{1}{m_2}\right) \tag{4-7}$$

Cross sections for process (4-1) have been obtained from the measured rate constants using Eqns. (4-5) and (4-7) and are given in Tables (4-1) to (4-7).

4.3 General theory for collisional ionization of high Rydbergs.

Theoretical investigations of the collisional ionization of high Rydbergs by molecules have proceeded along a number of paths. In one approach Matsuzawa has employed quantum mechanical scattering theory to examine process (4-1) for target molecules, BC, which non dissociatively capture electrons,[55] which dissociate upon electron capture,[56] and which possess dipole or quadrupole moments.[57,58] Flannery, in another approach, has applied the correspondence principle to the process and this has allowed him to construct a semiquantal theory for the ionization process at thermal energies.[59,60] Fowler and Preist[7] and Preist[8] have adopted to the present high Rydberg-molecule interaction a model used in describing collisions between elementary particles.

Each of the theories just mentioned is based on the fact that the Rydberg electron is at a very large distance from the Xe^+ core and has a small binding energy. From a quantum mechanical viewpoint the probability density of finding the electron at a given distance from the core reaches a maximum when this distance is very large. From a classical point of view, the electron describes an elliptical trajectory about the core and spends the

majority of its time around the far radial turning point of the orbit. In a collision between a high Rydberg atom and a target molecule, the Rydberg electron and the molecule can interact independently of the high Rydberg core. At such a great distance from the site of the electron-molecule interaction, the core plays no role in the collision except to define the velocity distribution of the Rydberg electron. This situation can be stated formally according to the following conditions given by Flannery.[60] First, the scattering lengths for the electron-core and the molecule-core systems are much smaller than the distance between the electron and the core. Second, the distance between the electron and the core greatly exceeds the reduced wavelength of the molecule. Third, the orbital period of the electron is much longer than the time interval over which the electron-molecule collision occurs. Finally, the collision time is also shorter than the vibrational period of the molecule. These conditions imply that the core and the electron are independent scattering centers which do not influence each other, that the consequence of the electron being bound is negligible as far as the electron-molecule collision is concerned, and that the molecule does not rotate during the collision. Concerning these conditions,

Flannery[60] has found that for a collision between a ground state hydrogen atom and a high Rydberg hydrogen atom having a principal quantum number of 100, the distance between the electron and the core is roughly three orders of magnitude larger than the two scattering lengths mentioned in the second condition. Matsuzawa[57] has also looked at the scattering length for the core-molecule system by examining the influence of the core on a molecule having a permanent multipole moment when the two are separated by the high Rydberg radius. He found the effects to be very small. These remarks indicate that the Rydberg electron can be considered to be essentially free and to be influenced by the core only in that its velocity distribution is determined by the core. It is this viewpoint, in which the Rydberg electron is regarded as free, that forms the cornerstone of the theories dealing with the collisional ionization of high Rydbergs. This model was first employed by Fermi[61] who calculated the displacements of Rydberg levels due to the presence of a foreign gas by considering the Rydberg electrons to freely scatter from the foreign gas molecules.

The application of the model just described requires the examination of the Rydberg electron-molecule collision which in turn necessitates a knowledge of the interaction

between an electron and a molecule. Although this interaction contains both short- and long-range terms,[62,63] only the asymptotic form appropriate to long-range encounters is used in the present application because, for the molecules so far investigated, the long-range terms are significant. For linear molecules, the leading terms of the asymptotic expression are proportional to

$$\frac{D}{r^2} P_1(\cos\theta), \quad \frac{Q}{r^3} P_2(\cos\theta), \quad \frac{\alpha}{r^4}, \quad \text{and} \quad \frac{\alpha'}{r^4} P_2(\cos\theta)$$

(see, for example, Refs. 60, 62, 63). Here, r is the electron-molecule separation, D and Q are the electric dipole and quadrupole moments respectively of the molecule, α and α' are the spherical and non-spherical components respectively of the molecular polarizability, and $P_n(\cos\theta)$ is a Legendre polynomial where θ is the angle between the molecular axis and $\vec{r}$.

4.4 Discussion of thermal electron attaching targets.

A number of experimental investigations have been conducted concerning the collisional ionization of high Rydbergs by molecules which capture free low energy electrons. Hotop and Niehaus[16] have measured absolute cross sections of $\approx 10^{-12}$ cm^2 for the reaction

$$A^{**} + SF_6 \rightarrow A^+ + (SF_6 + e) \qquad (4\text{-}8)$$

where A** is a He, Ne, or Ar high Rydberg formed by electron impact. Their results also indicate that the electron is captured by the SF_6. This reaction, for the case of xenon high Rydberg atoms in well defined states, has been studied in detail by West et al.[45] The rate constants and cross sections that they obtained are based on the Xe^+ ion production in the process and are in reasonable agreement with the cross sections of Hotop and Niehaus, just discussed.

SF_6 nondissociatively captures free thermal electrons.[64] Since the excited electron in a high Rydberg atom is viewed as being essentially free, according to the earlier discussion, and since it has an energy comparable to thermal energy due to its small binding energy, process (4-8) above can be explained as the Rydberg electron attaching to the target molecule. Matsuzawa[55] has supplied the details of this explanation. Using a projection operator approach, which is popular in the treatment of collision resonance phenomena, and ignoring the interaction between the high Rydberg core and the molecule, he shows that the scattering amplitude for the high Rydberg-molecule collision is related directly to the free thermal electron capture matrix element. This matrix

element is then rewritten in terms of the rate constant for thermal electron capture. From the scattering amplitude Matsuzawa calculates the cross section, averaged over the Rydberg electron's orbital angular momentum quantum numbers, for the high Rydberg-molecule collision. Finally, this cross section is used to obtain a rate constant, k_c, for the collision. The result is that this rate constant is equal to the rate constant, k_a, for the nondissociative capture of free electrons to the target molecule. This result applies under the condition that the electron attaches to the same negative ion state in both the high Rydberg-molecule collision and free electron-molecule collision. Based on this conclusion, that $k_c = k_a$, West et al.[45] have compared their results for k_c with those of experiments on the attachment of free thermal electrons to SF_6 and has shown that the two sets of data are in good accord. In addition the measurements of West et al. show an independence of the rate constant, k_c, from the principal quantum number of the Rydberg electron.

The above discussion has dealt with nondissociative electron attaching target gases. An alternative situation concerns target molecules which dissociate following capture of free thermal electrons such as CH_3I.[22] Stockdale

et al.[22] have detected the occurance of the reaction

$$Ar^{**} + CH_3I \rightarrow Ar^+ + CH_3 + I^- \qquad (4\text{-}9)$$

in electron swarm experiments and determined an upper limit to the rate constant of 8.9×10^{-7} $cm^3 sec^{-1}$. CCl_4 also dissociatively captures free thermal electrons. Evidence for

$$Kr^{**} + CCl_4 \rightarrow Kr^+ + Cl^- + CCl_3 \qquad (4\text{-}10)$$

was given by Melton and Hamill[11] in an analysis of ion appearance potentials for produced ions in an electron bombardment ion source. In the present work the rate constant for the process

$$Xe(nf) + CCl_4 \rightarrow Xe^+ + (CCl_4 + e) \qquad (4\text{-}11)$$

has been measured in field free conditions and the results are shown in Table (4-1) and in Fig. (4-1).

Matsuzawa[56] has given a theoretical treatment for the collisional ionization of high Rydbergs by targets which dissociate upon capture of free thermal electrons. This theory, based on the idea of the Rydberg electron being a slow, free electron which scatters off the target molecule, is a modification of the earlier analysis for nondissociating targets in order to allow for dissociation. In the nondissociating case, the negative ions formed are

long-lived resonances and their subsequent decay or stabilization can be ignored. In the present case the negative ions dissociate in a time comparable to a vibrational period and the final channel of the collision contains a neutral and a negative fragment of the original molecule. The capture process in this situation is separated into two steps: (1) capture of a free thermal electron to form the negative ion resonance, and (2) dissociation of this resonance. In Matsuzawa's theory the free electron is replaced by the Rydberg electron. Based on this model of the reaction, the expression derived in the earlier theory for the dependence of the scattering amplitude of the high Rydberg-molecule collision on the matrix element for free electron attachment can be adopted in the present theory as long as the matrix element is written for a dissociative capture process, i.e., as long as it allows for dissociation to occur. Manipulation of this scattering amplitude in a manner similar to the earlier theory produces the result that the rate constant, k_c, for the process

$$A(n) + CCl_4 \overset{k_c}{\rightarrow} A^+ + CCl_3 + Cl^- \qquad (4\text{-}12)$$

is equal to the rate constant, k_a, for the dissociative capture of free thermal electrons by CCl_4

$$e + CCl_4 \xrightarrow{k_a} CCl_3 + Cl^-. \qquad (4\text{-}13)$$

As was the case before, the negative ion formed in the high Rydberg-molecule collision must be the same as the ion produced in the free electron-molecule collision. Also as before, Matsuzawa has performed an average over the Rydberg electron's orbital angular momentum quantum numbers in deriving his result for k_c.

In view of the model used and with the conclusion that $k_c = k_a$, it is possible to compare the present experimental results for process (4-11) with the experimental swarm data of Bouby et al.,[65] Christodoulides and Christophorou,[66] and Davis et al.[67] for process (4-13), by plotting the data as a function of the electron energy regardless of whether it is a Rydberg or a free electron. This is shown in Fig. (4-11). The data for k_c from the high Rydberg collisions is plotted along the energy scale using the binding energy of the Rydberg electron which, by the Virial theorem, equals the time average of the electron's kinetic energy. It is seen that general agreement exists between the data even though there is no overlap in energy intervals covered by the two sets of data.

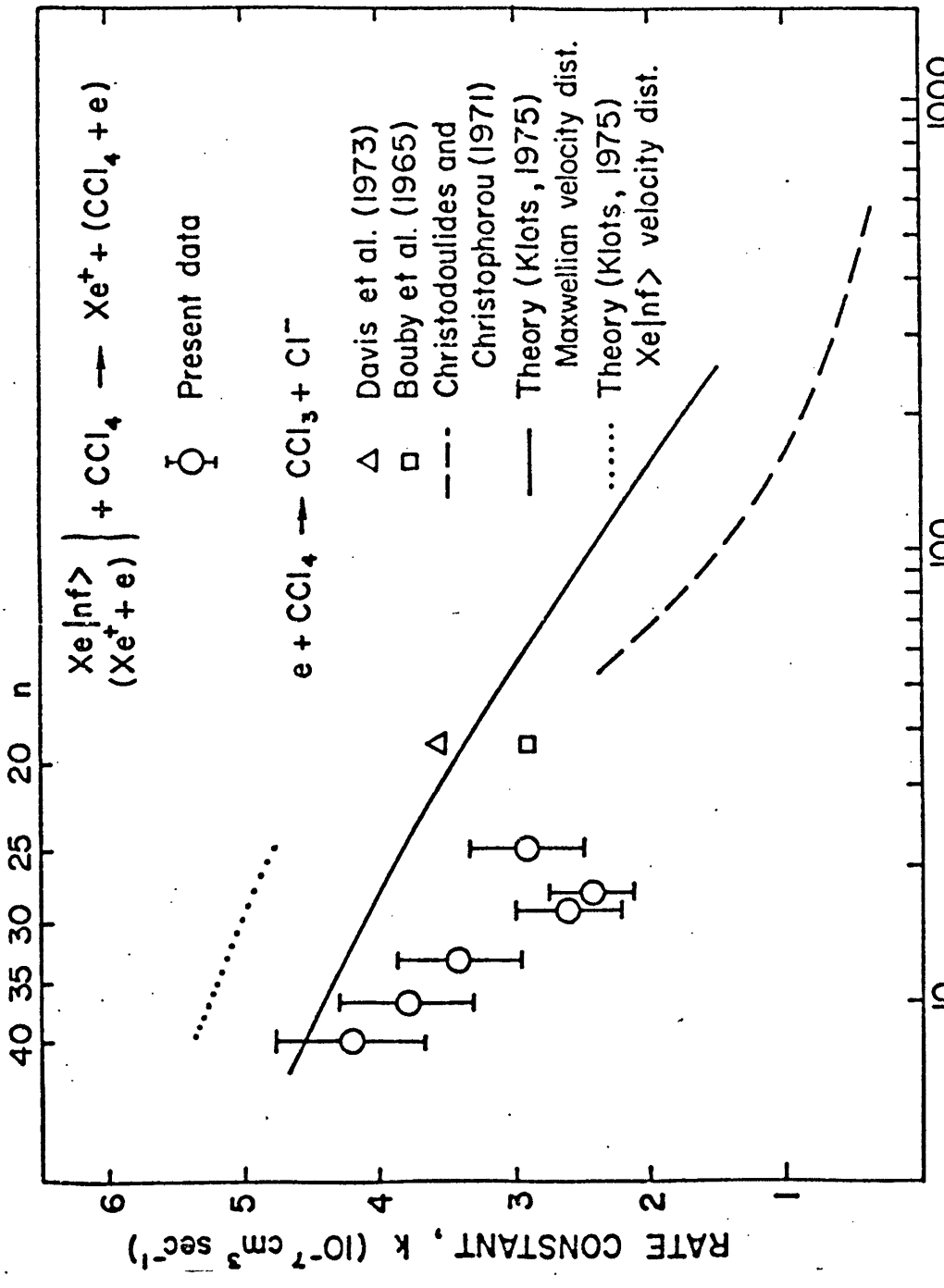

Figure (4-11) Comparison of the results for CCl_4 with experiment and theory.

Matsuzawa expresses the rate constant, k_c, for the collisional ionization of a high Rydberg by an electron attaching molecule in terms of the interaction between a free electron and the molecule. He then converts this interaction term into a rate constant, k_a, for the capture of free electrons by the molecule and therefore arrives at a useful relation between k_c and k_a. This theory does not, however, express k_c in terms of fundamental quantities.

The validity of the basic model of the collisional ionization of high Rydbergs-- viewing the Rydberg electrons as essentially free -- can be examined by comparing the rate constants measured in the present work, k_c, with rate constants, k_a, obtained from a theoretical cross section, $\sigma_a(v)$ given by Klots[68] for the attachment of free electrons to molecules. The cross section is based on the r^{-4} polarization potential that exists between an electron and a neutral molecule as discussed in Sec. 4.3, and is given by

$$\sigma_a(v) = \pi \lambda^2 [1 - \exp(-v\sqrt{\frac{8 \alpha m}{R a_o^3}})] \qquad (4\text{-}14)$$

where λ is the reduced wavelength of the relative motion between the electron and the molecule, α is the polarizability of the molecule, m is the electron's mass, R is the

Rydberg constant in eV, and a_o is the Bohr radius. Using the expression

$$k_a = \int \sigma_a(v)\ v\ f(v)\ dv \qquad (4\text{-}15)$$

where v and f(v) are the velocity and velocity distribution of the electron, a rate constant may be determined from $\sigma_a(v)$. At this point it is necessary to choose a velocity distribution f(v). This affords the opportunity to examine the degree to which different distributions, namely, the velocity distributions of the Rydberg electron and the free electron, affect the value of the rate constant. The solid line in Fig. (4-11) gives k_a from Eqn. (4-15) when f(v) is a Maxwellian velocity distribution and is more appropriate to the free electron data. The dotted line in Fig. (4-11) gives k_a when f(v) is the distribution of an nf Rydberg electron in an elliptical orbit. This distribution has been discussed by West.[51] The values of the rate constant determined with a Rydberg electron velocity distribution are plotted along the energy scale using the binding energy of the Rydberg electron (equal to the electron's time averaged kinetic energy) while the rate constants obtained from a Maxwellian f(v) are plotted using the rms velocity of the distribution.

Although the above results indicate that process (4-1) appears to be reasonably well understood for electron attaching targets, this is not entirely the case. On the basis of the theoretical explanations just given, one would not expect a target molecule, which does not have a significant cross section for capture of free thermal electrons, to ionize a high Rydberg atom by capturing the Rydberg electron either dissociatively or nondissociatively. This appears to be the case for CH_3Br which has a small free electron attachment rate.[22] However, Suguira and Arakawa,[19] Stockdale et al.,[22] and Shibata et al.[29] have detected CH_3CN^- in collisions between rare gas high Rydbergs and CH_3CN. CH_3CN does not have an appreciable low energy electron attachment cross section and its mode of production in the above reactions is currently unclear. For the molecule CH_3NO_2, Stockdale et al.[22] have measured an upper bound of $\sim 10^{-11}$ cm^2 for the cross section of the reaction

$$Ar^{**} + CH_3NO_2 \rightarrow Ar^+ + CH_3NO_2^- \qquad (4\text{-}16)$$

using a swarm technique and a time of flight analysis of the ions produced. Production of $CH_3NO_2^-$ ions was also observed in a reaction analogous to (4-16) in which krypton was used instead of argon.[22] This data indicates that

CH_3NO_2 would capture free thermal electrons nondissociatively. Such does not appear to be the case as NO_2^- and CN^- ions are the major products of low energy electron swarm experiments with CH_3NO_2.[22] The situation regarding this molecule is further complicated by the fact that it possesses a large dipole moment (see Sec. 4.5). CH_3CN and CH_3NO_2 are reasonable candidates for further study.

4.5 Discussion of dipole targets.

The ability of target molecules having permanent dipole moments to collisionally ionize high Rydbergs has also been investigated experimentally. Hotop and Niehaus[16] have measured cross sections for the reaction (4-1) where the high Rydberg, A**, was He, Ne, or Ar, while the target molecule was H_2O, NH_3, or SO_2. The cross sections measured ranged from 1.1×10^{-13} cm^2 to $1.2 \times 10^{-12} cm^2$. In the present work the process

$$Xe(nf) + BC \rightarrow Xe^+ + (BC + e) \qquad (4\text{-}17)$$

is studied where BC is H_2O, NH_3, H_2S, or SO_2. The absolute rate constants measured are given along with the cross sections in Tables (4-2) through (4-5) for the various target gases. The results of Hotop and Niehaus[16] are also given for comparison. Considering that the values

of Hotop and Niehaus are for high Rydbergs having a large mixture of n values and were obtained in an electric field of ~100 V/cm (see Sec. 4.7), reasonable agreement is evident. The rate constants have been plotted against n in Figs. (4-2) and (4-3) and a composite logarithmic graph of the results is shown in Fig. (4-12). It is seen that the cross sections are rather rapidly increasing functions of n. The geometric cross section of the Xe(nf) atom, which scales as n^4 is also given for comparison.

Theoretical explanations for the ionization of high Rydbergs by dipole and quadrupole molecules have been advanced by Matsuzawa,[57,58] Flannery,[60] and Preist.[8] These theories rely on the assumption that the Rydberg electron is essentially free, has a low energy, and scatters off the molecule independently of the high Rydberg core. From the discussion in Sec. 4.3, the interaction between the electron and the molecule consists either of the dipole or the quadrupole term depending on the target. These interactions give rise to inelastic and superelastic collisions in which the rotational state of the molecule is changed. In the present collisional situation the analysis is based on the premise that a superelastic collision occurs between the electron and the molecule in

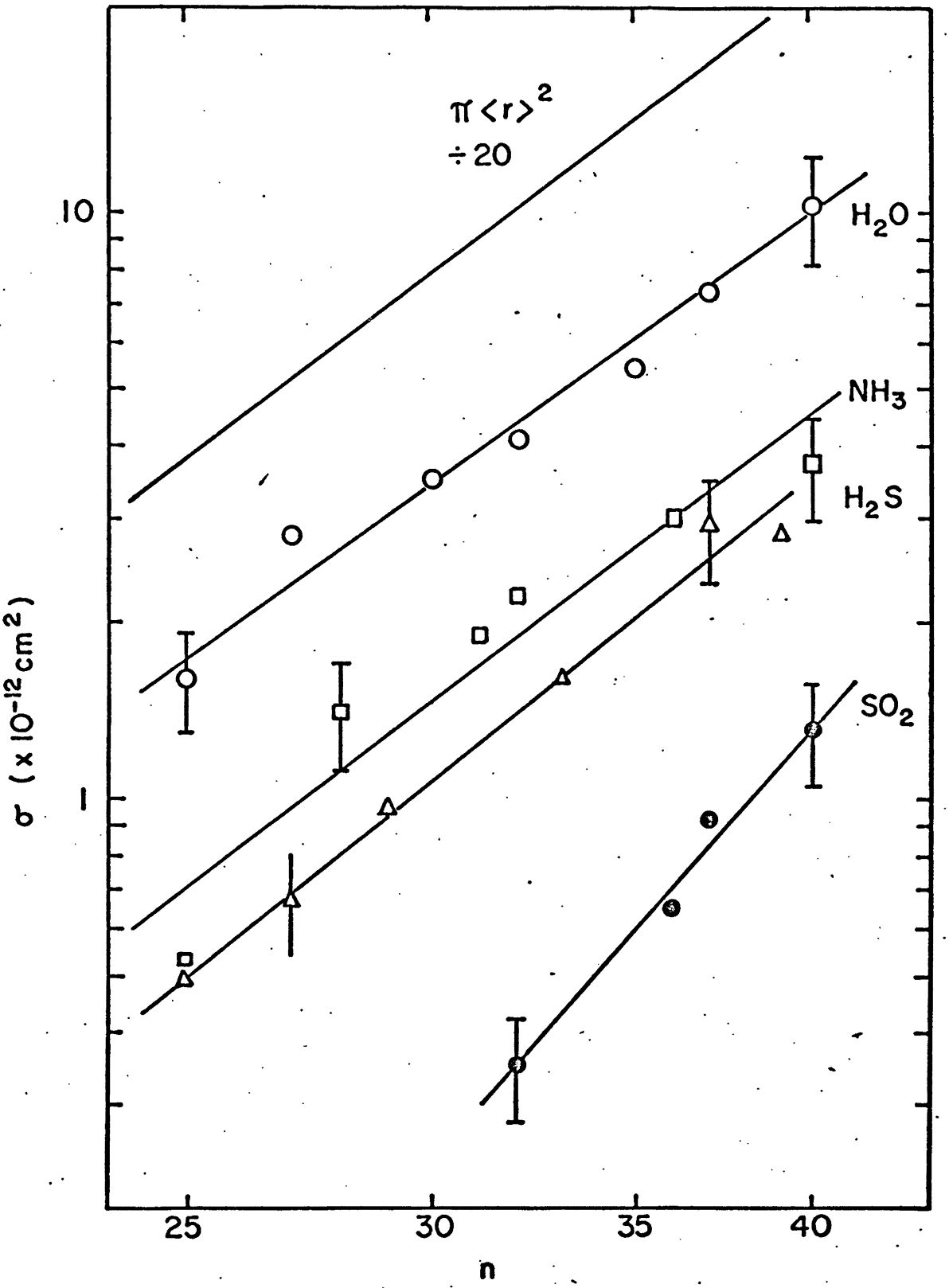

Figure (4-12) Composite of the results for the dipole targets; comparison with Xe(nf) geometric cross section.

which the molecule is rotationally de-excited. The energy released from this de-excitation is transferred to the electron. An additional constraint must be placed on this scattering process in order for it to be applied to the present high Rydberg ionization process. The rotational de-excitation must release enough energy to ionize the high Rydberg, i.e., the released energy must exceed the binding energy of the Rydberg electron. (Flannery actually discusses the more general case of n changing collisions which include the ionization possibility.) Rotational excitation and de-excitation of molecules by electron impact has received a good deal of attention in the past and is currently a popular subject.

Matsuzawa calculates the scattering amplitude for the high Rydberg-molecule collision using a matrix element over the Rydberg electron-molecule interaction. This matrix element connects an initial state, which is the product of the electronic and molecular wavefunctions, and a final state consisting of an asymptotic scattering state of the Hamiltonian belonging to the entire high Rydberg-molecule system. After some manipulation, the matrix element can be expressed in terms of the scattering amplitude of a free electron colliding with the molecule. The free electron scattering amplitude is then calculated

for a charge interacting with a point multipole in the Born approximation making use of the electron-molecule scattering results of several earlier investigators. This calculation depends on the target molecule involved since both the kinds of rotational transitions that are allowed (i.e., the selection rules on rotational quantum numbers) and the amount of energy released in the rotational transition (i.e., the spacing between the rotational energy levels) depend on the molecule's structure. Molecules can be classified according to their structure into various rotational types. These types can be described either in terms of the moments of inertia about the three principal axes of rotation of the molecule, I_A, I_B, and I_C, or they can be described in terms of the molecule's rotational constants, A, B, and C, which are defined as

$$A = \frac{h}{8\pi^2 c I_A} \qquad B = \frac{h}{8\pi^2 c I_B} \qquad C = \frac{h}{8\pi^2 c I_C} . \quad (4\text{-}18)$$

Using A, B and C, the rotational types include: linear molecules ($A = 0$, $B = C \neq 0$); prolate symmetric top molecules ($A > B = C$); oblate symmetric top molecules ($A = B > C$); and, asymmetric top molecules ($A > B > C$).[69] For a dipole molecule the selection rule on the total rotational angular momentum quantum number, J, is $\Delta J = 1$. It should be pointed out that the general format used by

Matsuzawa, i.e., casting the high Rydberg-molecule collision in terms of a free electron-point multipole scattering process for which the Born approximation calculations of other workers are employed, is also followed by Flannery[60] and Preist.[8] On the basis of this model, Eqn. (4-1) may be written for dipole target molecules

$$A^{**} + BC(J) \rightarrow A^{+} + BC(J-1) + e \qquad J \geq J_o \qquad (4\text{-}19)$$

where J_o specifies the lowest rotational state from which a $\Delta J = 1$ transition will release sufficient energy to ionize the high Rydberg.

For the final result of the collisional ionization of a high Rydberg by a dipole molecule, Matsuzawa gives the cross section

$$\sigma_c = 4.7\ \mu^{1/2}\ D^2\ \langle I_d \rangle \times 10^{-13}\ cm^2 \qquad (4\text{-}20)$$

where μ is the reduced mass of the system in a.m.u., D is the dipole moment of the molecule atomic units, and $\langle I_d \rangle$ is a dimensionless quantity which depends on the type of molecule involved and on the molecule's rotational constants. $\langle I_d \rangle$ is derived from an earlier quantity which depended on the principal quantum number, n, of the high Rydberg and the rotational quantum numbers of the molecule,

in addition to the type of molecule and the molecule's rotational constants. The brackets, < >, indicate an average over the value of n using an n^{-3} weighting factor and over the allowed values of the rotational quantum numbers.

Comparison of the present experimental data with the theoretical results is given in Fig. (4-13) by plotting σ_c against $\mu^{1/2} D^2 \langle I_d \rangle$. Matsuzawa's results are given for SO_2, NH_3, H_2O, and CH_3NO_2. Due to the fact that the rotational constants B and C of SO_2 are almost equal when compared to the other constant, A, Matsuzawa has approximated SO_2 as a prolate symmetric top molecule. In addition, he has used the oblate symmetric top classification for CH_3NO_2. The theoretical H_2S point is determined from Eqn. (4-20) assuming a value of 2.9 for $\langle I_d \rangle_{H_2S}$. The present experimental results are given for n = 25, n = 32, and n = 40. The comparison is extended in Fig. (4-14) which shows the theoretical results again along with the present experimental results for each gas, this time, averaged over n using the n^{-3} weighting factor as follows

$$\bar{\sigma} = \frac{\sum_n \sigma_n n^{-3}}{\sum_n n^{-3}} . \qquad (4\text{-}21)$$

Here the summation extends only over values of n for for which the cross sections for the particular gas were measured. It is seen that the agreement is very good. The molecular constants and other quantities that are important in the present analysis are given in Table (4-8).

It is seen from Figs. (4-12) through (4-14) that the cross sections increase with increasing D in accordance with Eqn. (4-20) for all gases except SO_2. The reason for this exception lies in the very small rotational constants that SO_2 possesses, due to the following reason. Since rotational level separation increases with increasing J and since ΔJ can only be unity, it is seen that in order for a molecule to be efficient in the ionization process it must possess rotational levels that lie high enough in energy to provide the necessary ionization energy and yet remain significantly populated at room temperature. This structure is determined by the rotational constants of the molecule. With such small separation between rotational levels in SO_2 it is necessary to go to quite high values of J to achieve sufficient energy in a $\Delta J = 1$ transition to ionize the high Rydberg. At such high J values there is no longer a significant population of the levels. In the theory this feature appears as a small value of $\langle I_d \rangle_{SO_2}$. CH_3NO_2 also has small rotational constants

Table 4-8

Quantities for Dipole Targets

	$D^{\dagger}$ (a.u.)	$A^{\#}$ (cm^{-1})	$B^{\#}$ (cm^{-1})	$C^{\#}$ (cm^{-1})	$\mu^{1/2} D^2 < I_d >$	σ Theory (10^{-12} cm^2)	σ Exp. Ave. (10^{-12} cm^2)
CH_3NO_2	1.36		0.35	0.20	7.00	3.29	
H_2O	0.727	27.88	14.51	9.29	6.96	3.27	3.85
SO_2	0.641	2.03	0.34	0.29	1.46	6.84	0.723
NH_3	0.578		9.44	6.20	2.83	1.33	1.66
H_2S	0.38	10.37	8.99	4.73	2.13 ##	1.0 ##	1.15

† Values for CH_3NO_2, H_2O, SO_2, and NH_3 taken from Ref. 58; value for H_2S taken from Ref. 70

\# Values for CH_3NO_2, H_2O, SO_2, and NH_3 taken from Ref. 58; value for H_2S taken from Ref. 69

Calculated using $<I_d>_{H_2S} = 2.9$ (see page 97)

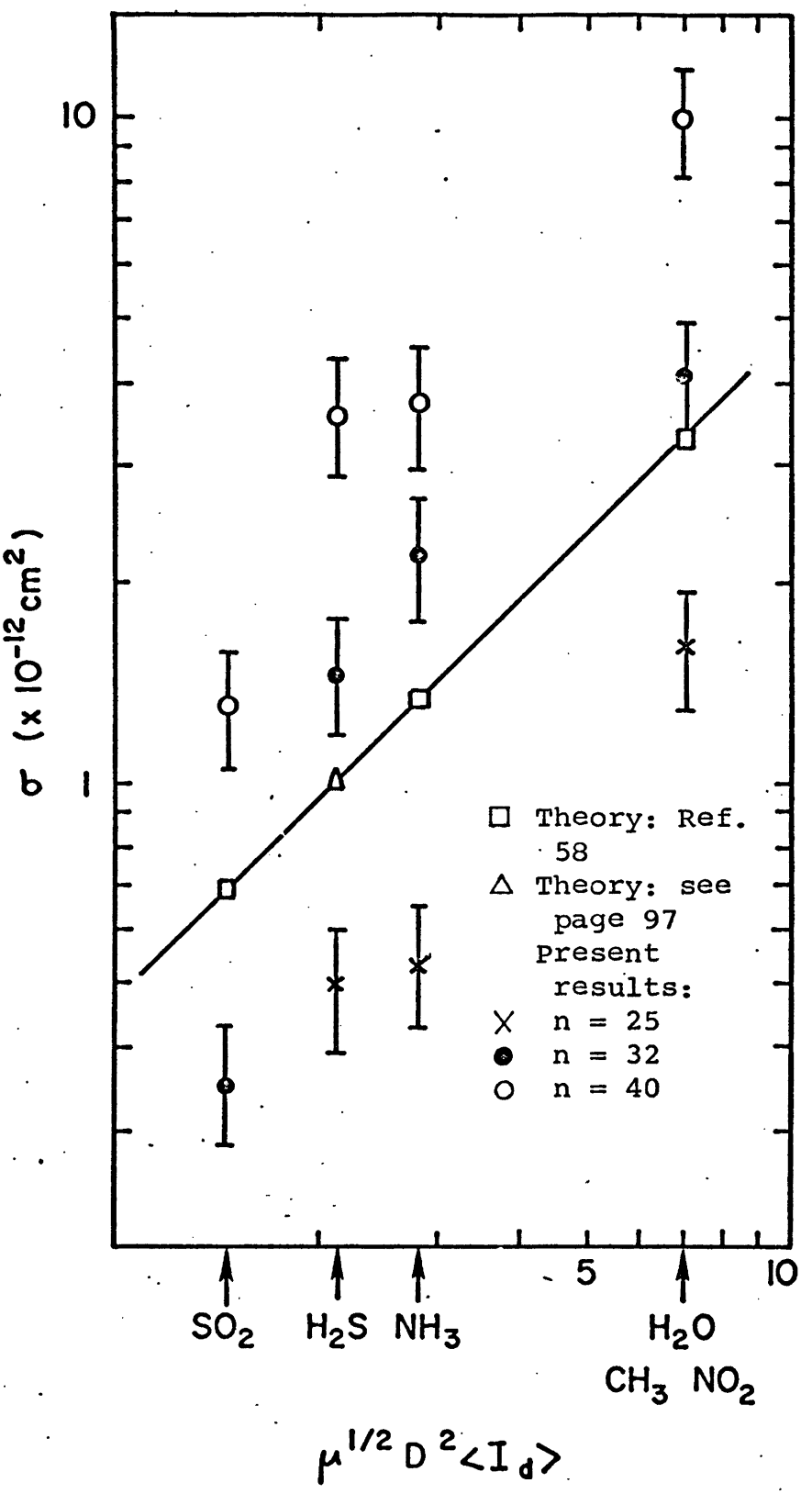

Figure (4-13) Comparison of the results for the dipole targets with theory.

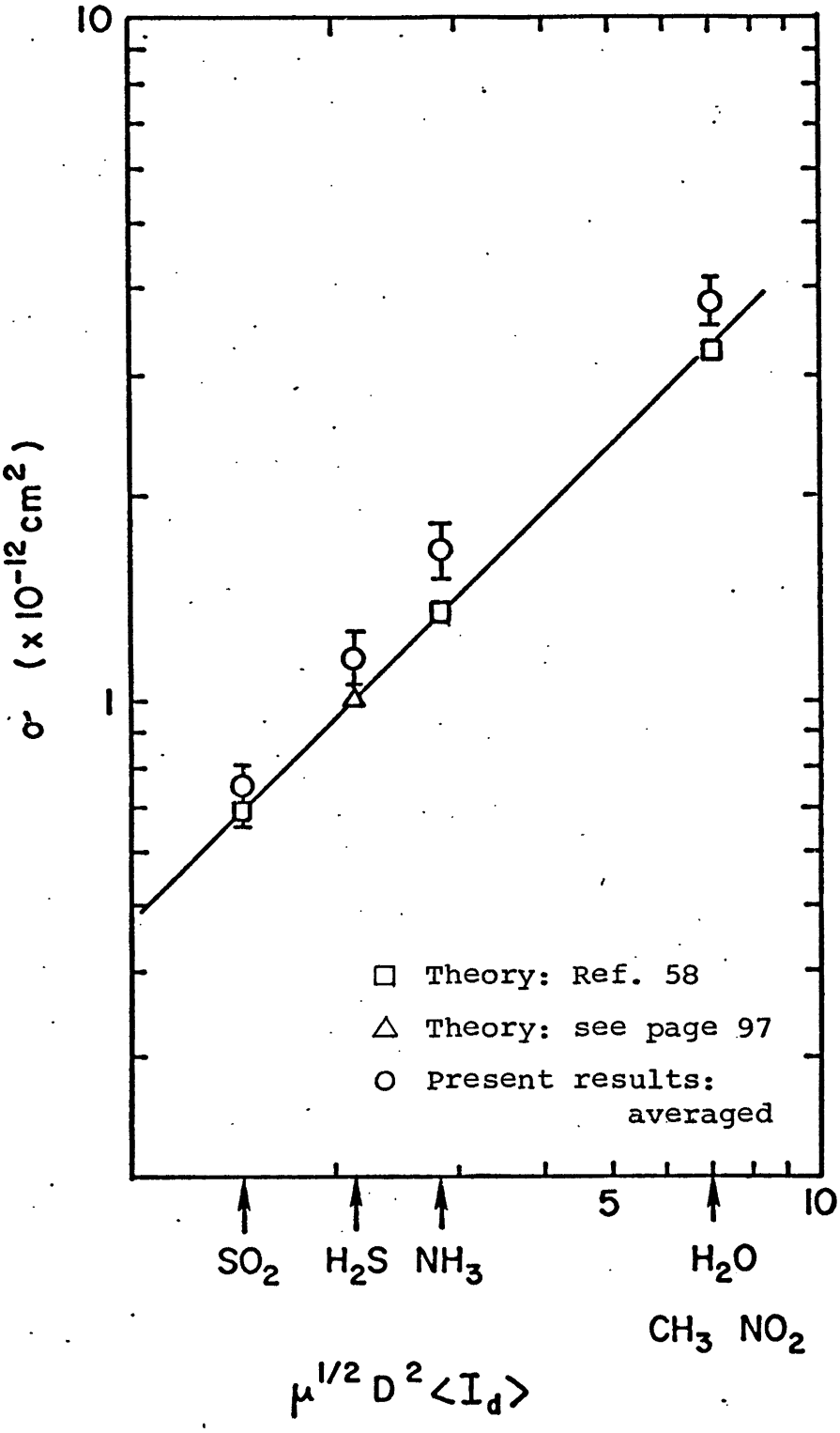

Figure (4-14) Comparison of the averaged results for the dipole targets with theory.

and the discussion just given explains why the theoretical cross section for CH_3NO_2 is smaller -- nearly equal to that of H_2O [see Fig. (4-13)] -- than would be indicated by a comparison of the dipole moments alone of CH_3NO_2 and H_2O.

It is also reasonable to assume for a large enough range of n that the collisional ionization cross section will have a step structure as a function of n, due to successive rotational levels entering into the process as n changes. This step structure is not visible in the present results. This is presumably due to the fact that the molecules studied have more than one spectrum of rotational levels and, although each series of levels may produce the step phenomenon, the combination of all the series averages out this feature. This step structure would be most evident for diatomic target gases.

4.6 Discussion of CCl_3F and CCl_2F_2.

The data obtained in the present experiment for collisions between CCl_3F and Xe(nf) high Rydbergs are given in Table (4-6) and Fig. (4-4). CCl_3F has a significant cross section for the dissociative capture of free thermal electrons and, in addition, has a dipole moment. It is reasonable to expect that in a collision between a high Rydberg and CCl_3F both collisional ionization by

dissociative electron attachment to CCl_3F and rotational de-excitation of CCl_3F will play a role. In an attempt to determine which process is more important, collisions between CCl_2F_2 and Xe(nf) high Rydbergs were also studied. These data are given in Table (4-7) and Fig. (4-5). CCl_2F_2 does not capture free thermal electrons but it has a dipole moment similar to CCl_3F and the rotational structure of CCl_2F_2 might be expected to be similar to that of CCl_3F. Fig. (4-15) shows a comparison of the results for CCl_4, CCl_3F, and CCl_2F_2. A conclusion that may be drawn from this figure is that process (4-19) is not very significant in collisions between CCl_3F and high Rydbergs.

4.7 Discussion of electric field effect on k_c.

The effect of a small electric field on the rate constant for collisional ionization of Xe(nf) atoms with the target gases CCl_4, H_2O, NH_3, H_2S, and CCl_3F has been examined in the present work and the results are shown in Figs. (4-6) through (4-10). An observable decrease in k_c is evident for CCl_4 and CCl_3F, while no effect is exhibited for the other targets within the present detectability limits.

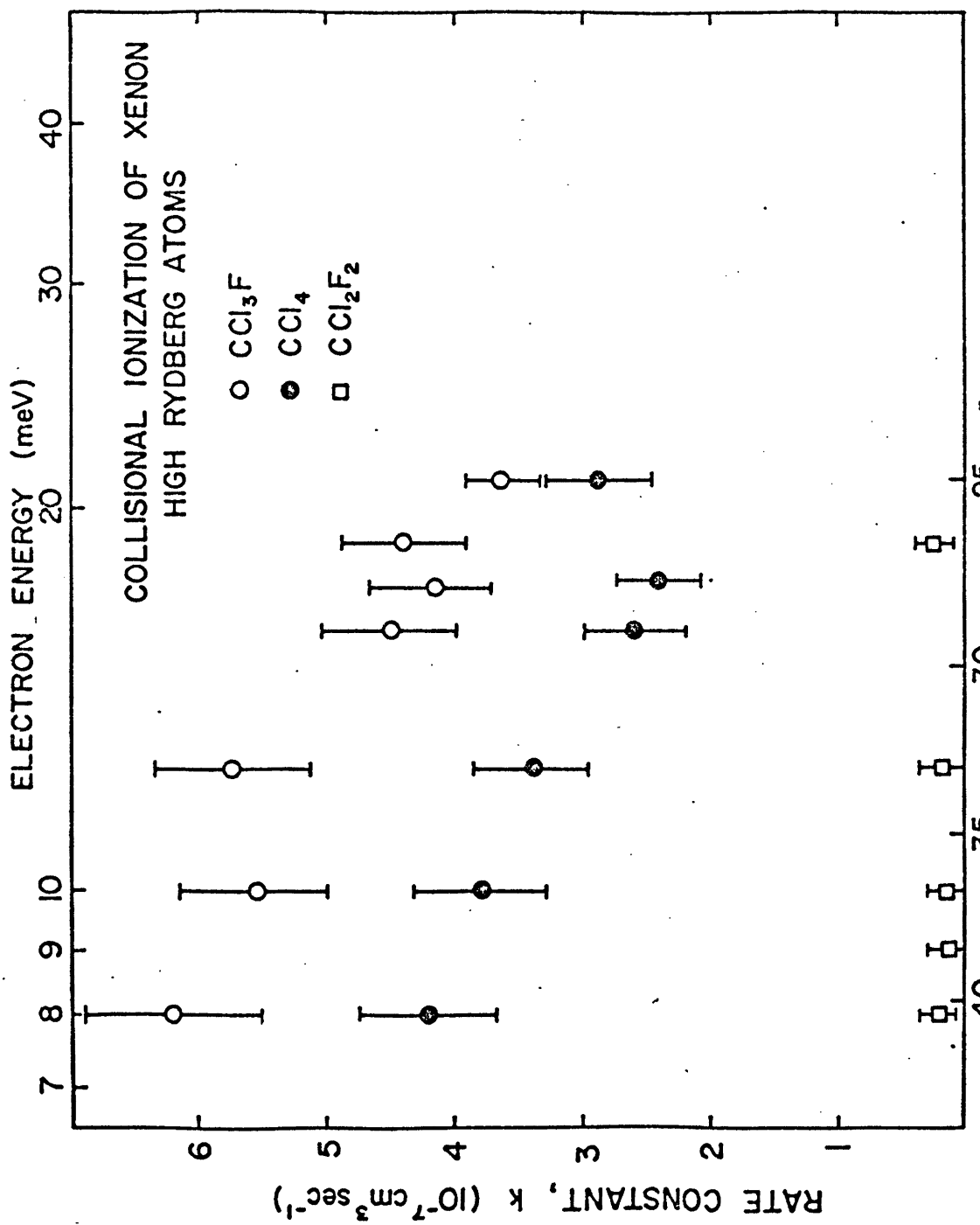

Figure (4-15) Comparison of the results for CCl_4, CCl_3F, and CCl_2F_2.

BIBLIOGRAPHY

1. A. K. Dupree and L. Goldberg, in Ann. Rev. Astr. Astrophys. 8, 231, 1970
2. M. J. Seaton, in Adv. Atom. Mol Phys. 4, 331, 1968; in Atoms and Molecules in Astrophysics, ed. T. K. Carson and M. J. Roberts, 1972, p. 121
3. I. C. Percival, in Atoms and Molecules in Astrophysics, eds. T. K. Carson and M. J. Roberts, 1972, p. 65
4. D. R. Bates, A. E. Kingston, and R. W. P. McWhirter, Proc. Roy. Soc. A267, 297, 1962; A270, 155, 1962
5. R. W. P. McWhirter and A. G. Hearn, Proc. Phys. Soc. 82, 641, 1963
6. J. R. Hiskes, Nucl. Fusion 2, 38, 1962
7. G. N. Fowler and T. W. Preist, J. Chem. Phys. 56, 1601, 1972
8. T. W. Preist, J. Chem. Soc. Farad. Trans. I, 68, 661, 1972
9. R. V. Ambartsumyan, G. I. Bekov, V. S. Letokhov, and V. I. Mishin, JETP Lett. 21, 279, 1975
10. V. Cermak and Z. Herman, Coll. Czechoslov. Chem. Commun. 29, 953, 1964
11. C. E. Melton and W. H. Hamill, J. Chem. Phys. 41, 1469, 1964

12. S. E. Kupriyanov, Sov. Phys. - JETP 21, 311, 1965

13. S. E. Kupriyanov, Opt. Spectrosc. 20, 85, 1966

14. S. E. Kupriyanov, Sov. Phys. - JETP 24, 674, 1967

15. S. E. Kupriyanov, JETP Lett. 5, 197, 1967

16. H. Hotop and A. Niehaus, J. Chem. Phys. 47, 2506, 1967

17. H. Hotop and A. Niehaus, Z. Physik 215, 395, 1968

18. G. A. Surskii and S. E. Kupriyanov, Sov. Phys. - JETP 27, 61, 1968

19. T. Sugiura and K. Arakawa, in Recent Developments in Spectroscopy, Proc. Intern. Conf. Mass Spectroscopy (Kyoto) 1969, eds. K. Ogata and T. Haykawa, 1970, p. 848

20. T. Shibata, T. Fukuyama, and K. Kuchitsu, Mass Spectroscopy 21, 217, 1973

21. T. Shibata, T. Fukuyama, and K. Kuchitsu, Bull. Chem. Soc. Japan, 47, 2883, 1974

22. J. A. Stockdale, F. J. Davis, R. N. Compton, and C. E. Klots, J. Chem. Phys. 60, 4279, 1974

23. D. E. Donohue, J. A. Schiavone, D. R. Herrick, and R. S. Freund, Bull. Am. Phys. Soc. 20, 1458, 1975

24. S. E. Kupriyanov, Sov. Phys. - JETP 28, 240, 1969

25. R. S. Freund, J. Chem. Phys. 54, 3125, 1971

26. C. E. Fairchild, Bull. Am. Phys. Soc. 17, 132, 1972

27. K. C. Smyth, J. A. Schiavone, and R. S. Freund, J. Chem. Phys. 59, 5225, 1973

28. T. Shibata, T. Fukuyama, and K. Kuchitsu, Chem. Lett., 75, 1974

29. T. Shibata, T. Fukuyama, and K. Kuchitsu, Bull. Chem. Soc. Japan 47, 2573, 1974

30. K. C. Smyth, J. A. Schiavone, and R. S. Freund, J. Chem. Phys. 60, 1358, 1974

31. J. A. Schiavone, K. C. Smyth, and R. S. Freund, J. Chem. Phys. 63, 1043, 1975

32. W. C. Wells, W. L. Borst, and E. C. Zipf, in Electronic and Atomic Collisions, Abstracts IX ICPEAC (Seattle) 1975, eds. J. S. Risley and R. Geballe, 1975, p. 818

33. A. C. Riviere and D. R. Sweetman, in Atomic Collision Processes, Proc. III ICPEAC (London) 1963, ed. M. R. C. McDowell, 1964, p. 734

34. R. N. Il'in, B. I. Kikiani, V. A. Oparin, E. S. Solov'ev, and N. V. Fedorenko, Sov. Phys. - JETP 20, 835, 1965

35. J. E. Bayfield and P. M. Koch, Phys. Rev. Lett. 33, 258, 1974

36. P. M. Koch and J. E. Bayfield, Phys. Rev. Lett. 34, 448, 1975

37. R. E. Huffman and D. H. Katayama, J. Chem. Phys. 45, 138, 1966

38. W. A. Chupka, Bull. Am. Phys. Soc. 19, 70, 1974

39. T. F. Gallagher, S. A. Edelstein, and R. M. Hill, Phys. Rev. A 11, 1504, 1975

40. T. F. Gallagher, S. A. Edelstein, and R. M. Hill, Phys. Rev. Lett. 35, 644, 1975

41. T. W. Ducas, M. G. Littman, R. R. Freeman, and D. Kleppner, Phys. Rev. Lett. 35, 366, 1975

42. M. G. Littman, M. L. Zimmerman, T. W. Ducas, R. R. Freeman, and D. Kleppner, Phys. Rev. Lett. 36, 788, 1976

43. T. B. Cook, W. P. West, F. B. Dunning, and R. F. Stebbings, Bull. Am. Phys. Soc. 20, 253, 1975

44. R. F. Stebbings, C. J. Latimer, W. P. West, F. B. Dunning, and T. B. Cook, Phys. Rev. A 12, 1453, 1975

45. W. P. West, G. W. Foltz, F. B. Dunning, C. J. Latimer, and R. F. Stebbings, Phys. Rev. Lett. 36, 854, 1976

46. P. M. Koch, L. D. Gardner, and J. E. Bayfield, to be published

47. H. A. Bethe and E. E. Salpeter, Quantum Mechanics of One- and Two-Electron Atoms, (Springer-Verlag) 1957, p. 262-269

48. L. Allen, D. G. C. Jones, and D. G. Schofield, J. Opt. Soc. Am. 59, 842, 1969

49. A. C. Riviere, Methods of Experimental Physics, eds. B. Bederson and W. L. Fite, 1968, vol. 7A, p. 208; R. N. Il'in, Atomic Physics 3, Proc. III ICAP (Boulder) 1972, eds. S. J. Smith and G. K. Walters, 1973, p. 309

50. A. V. Chaplik, Sov. Phys. - JETP 27, 178, 1968

51. W. P. West, Ph.D. thesis (Rice University, Houston) 1975

52. T. W. Hänsch, Appl. Opt. 11, 895, 1972

53. G. Loriot and T. Moran, Rev. Sci. Instrum. 46, 140, 1975; N. G. Utterback and T. Griffith, Jr., Rev. Sci. Instrum. 37, 866, 1966

54. R. D. Rundel, F. B. Dunning, and R. F. Stebbings, Rev. Sci. Instrum. 45, 116, 1974

55. M. Matsuzawa, J. Phys. Soc. Japan 32, 1088, 1972

56. M. Matsuzawa, J. Phys. Soc. Japan 33, 1108, 1972

57. M. Matsuzawa, J. Chem. Phys. 55, 2685, 1971

58. M. Matsuzawa, J. Elect. Spect. Rel. Phen. 4, 1, 1974

59. M. R. Flannery, Ann. Phys. (New York) 61, 465, 1970

60. M. R. Flannery, Ann. Phys. (New York) 79, 480, 1973

61. E. Fermi, Nuovo Cimento 11, 157, 1934

62. K. Takayanagi, J. Phys. Soc. Jap. 21, 507, 1966

63. K. Takayanagi, in Atomic Physics 4, Proc. 4th ICAP (Heidelberg) 1975, eds. G. zu Putlitz, E. W. Weber, and A. Winnacker, 1975, p. 435

64. F. C. Fehsenfeld, J. Chem. Phys. 53, 2000, 1970; L. G. Christophorou, D. L. McCorkle, and J. G. Carter, J. Chem. Phys. 54, 253, 1971

65. L. Bouby, F. Fiquet-Fayard, and H. Abgrall, C. R. Acad. Sci. Paris 261, 4059, 1965

66. A. A. Christodoulides and L. G. Christophorou, J. Chem. Phys. 54, 4691, 1971

67. F. J. Davis, R. N. Compton, and D. R. Nelson, J. Chem. Phys. 59, 2324, 1973

68. C. E. Klots, Chem. Phys. Lett. 38, 61, 1976

69. G. Herzberg, Molecular Spectra and Molecular Structure, Vol. I, Spectra of Diatomic Molecules, 2nd edition, Van Nostrand Reinhold Co., 1950; Vol. III, Electronic Spectra and Electronic Structure of Polyatomic Molecules, Van Nostrand Reinhold Co., 1966

70. CRC Handbook of Chemistry and Physics, 53rd edition, ed. R. C. Weast, The Chemical Rubber Co., 1972, p. E-51